Cell Reports

Article

Bisphosphoglycerate Mutase Deficiency Protects against Cerebral Malaria and Severe Malaria-Induced Anemia

Graphical Abstract

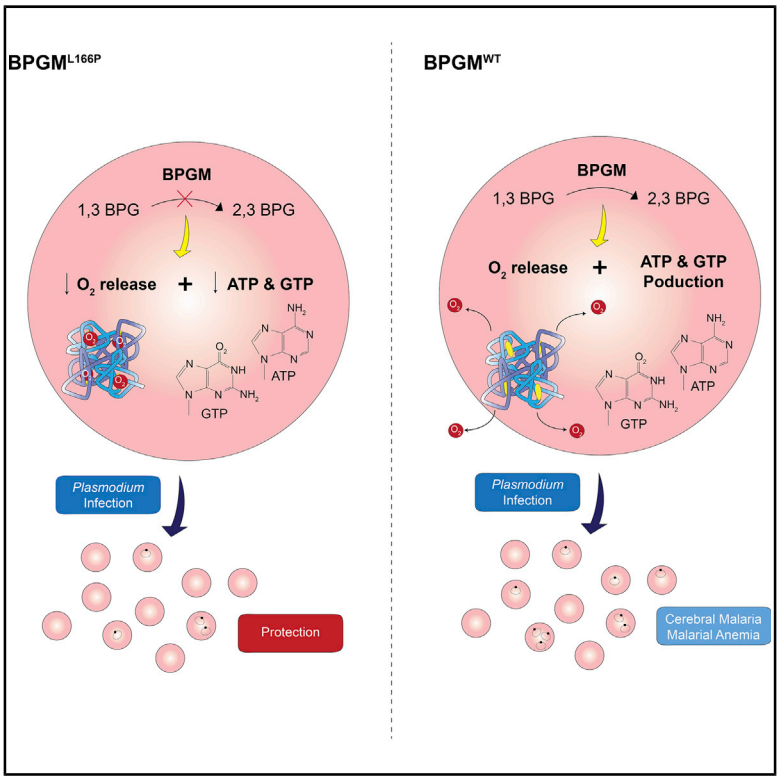

Highlights

- Inactivation of BPGM protects against malaria
- Protection is linked to increased erythropoiesis after parasite-induced hemolysis
- Reduced ATP levels in mutant erythrocytes reduces parasite replication

Authors

Guoyue Xu, Rebekah van Bruggen, Christian O. Gualtieri, ..., Silvia M. Vidal, Nassima Fodil, Philippe Gros

Correspondence

nassima.fodil@mcgill.ca (N.F.), philippe.gros@mcgill.ca (P.G.)

In Brief

Susceptibility to malaria is influenced by host genetics. Xu et al. demonstrate that a mutation in erythrocyte bisphosphoglycerate mutase protects against *Plasmodium* infection. Resistance involves both increased erythropoiesis in response to rising parasitemia and hemolysis and reduced intra-erythrocytic parasite replication associated with decreased energy metabolism with low ATP levels.

Xu et al., 2020, Cell Reports *32*, 108170
September 22, 2020
https://doi.org/10.1016/j.celrep.2020.108170

CellPress

Cell Reports

CellPress
OPEN ACCESS

Article

Bisphosphoglycerate Mutase Deficiency Protects against Cerebral Malaria and Severe Malaria-Induced Anemia

Guoyue Xu,[1,2] Rebekah van Bruggen,[2,3] Christian O. Gualtieri,[2,3] Neda Moradin,[2] Adrien Fois,[4,5] Diane Vallerand,[6] Mariana De Sa Tavares Russo,[7] Angelia Bassenden,[3] Wenyun Lu,[8] Mifong Tam,[9] Sylvie Lesage,[4,5] Hélène Girouard,[6] Daina Zofija Avizonis,[7] Geneviève Deblois,[10,11] Josef T. Prchal,[12] Mary Stevenson,[9] Albert Berghuis,[3] Tom Muir,[8,13] Joshua Rabinowitz,[8,13] Silvia M. Vidal,[1,2,9] Nassima Fodil,[2,14,*] and Philippe Gros[1,2,3,15,*]

[1]Department of Human Genetics, McGill University, Montreal, QC H3A 0C7, Canada
[2]McGill University Research Centre on Complex Traits, McGill University, Montreal, QC H3G 0B1, Canada
[3]Department of Biochemistry, McGill University, Montreal, QC H3A 1A3, Canada
[4]Immunology-Oncology Unit, Maisonneuve-Rosemont Hospital Research Center, Montréal, QC H1T 2M4, Canada
[5]Département de Microbiologie, Infectiologie et Immunologie, Université de Montréal, Montréal, QC H3T 1J4, Canada
[6]Université de Montréal, Département de Pharmacologie et Physiologie, Pav Roger-Gaudry, 2900 Édouard-Montpetit, Montréal, QC H3T 1J4, Canada
[7]Rosalind and Morris Goodman Cancer Research Centre, 1160 Pin Avenue West, Montréal, QC H3A 1A3, Canada
[8]Lewis Sigler Institute for Integrative Genomics, Princeton University, Princeton, NJ 08544, USA
[9]Department of Microbiology and Immunology, McGill University, Montréal, QC H3A 2B4, Canada
[10]Institute for Research in Immunology and Cancer, Université de Montréal, Montréal, QC H3T 1J4, Canada
[11]Faculté de Pharmacie, Université de Montréal, Montréal, QC H3C 3J7, Canada
[12]Division of Hematology, School of Medicine, University of Utah, Salt Lake City, UT 84132, USA
[13]Department of Chemistry, Princeton University, Princeton, NJ 08544, USA
[14]Centre CERMO-FC Pavillon des Sciences Biologiques, 141 Avenue du Président Kennedy, Montréal, QC H2X 3Y7, Canada
[15]Lead Contact
*Correspondence: nassima.fodil@mcgill.ca (N.F.), philippe.gros@mcgill.ca (P.G.)
https://doi.org/10.1016/j.celrep.2020.108170

SUMMARY

The replication cycle and pathogenesis of the *Plasmodium* malarial parasite involves rapid expansion in red blood cells (RBCs), and variants of certain RBC-specific proteins protect against malaria in humans. In RBCs, bisphosphoglycerate mutase (BPGM) acts as a key allosteric regulator of hemoglobin/oxyhemoglobin. We demonstrate here that a loss-of-function mutation in the murine *Bpgm* ($Bpgm^{L166P}$) gene confers protection against both *Plasmodium*-induced cerebral malaria and blood-stage malaria. The malaria protection seen in $Bpgm^{L166P}$ mutant mice is associated with reduced blood parasitemia levels, milder clinical symptoms, and increased survival. The protective effect of $Bpgm^{L166P}$ involves a dual mechanism that enhances the host's stress erythroid response to *Plasmodium*-driven RBC loss and simultaneously alters the intracellular milieu of the RBCs, including increased oxyhemoglobin and reduced energy metabolism, reducing *Plasmodium* maturation, and replication. Overall, our study highlights the importance of BPGM as a regulator of hemoglobin/oxyhemoglobin in malaria pathogenesis and suggests a new potential malaria therapeutic target.

INTRODUCTION

Malaria is a severe threat to global health, with an estimated 200 million cases and >400,000 deaths annually (World Health Organization, 2018). Malaria is caused by infection with different species of the protozoan parasite *Plasmodium* (*P. falciparum*, *P. malariae*, *P. ovale*, and *P. vivax*), with *P. falciparum* being the deadliest (Cowman et al., 2016; de Koning-Ward et al., 2016; White et al., 2014). The clinical symptoms of malaria occur at the blood stage, when the parasites replicate rapidly and lyse red blood cells (RBCs), causing anemia and high fever that can be severe (SMA [severe malarial anemia]). In addition, cytoadherent parasitized RBC (pRBC) can accumulate in brain capillaries that cause obstruction of blood flow and inflammation *in situ*; this cerebral malaria (CM) syndrome is the most lethal form of the disease (de Koning-Ward et al., 2016; Mishra and Newton, 2009; Rasti et al., 2004). Combined, SMA and CM represent the most severe malaria-associated cause of morbidity and mortality (Rasti et al., 2004).

Malaria is a striking example of human genetic effects in susceptibility to a lethal infection. Genetic studies in human populations have established the malaria-protective effect of several RBC-specific protein variants (Huang et al., 2018; Langlais et al., 2017; Torre et al., 2018). A clear example is the protective

effect of hemoglobin (Hb) alleles linked to sickle cell anemia (HbS) or thalassemias (HbC, HbE); although homozygosity for mutant HbS alleles causes life-threatening anemia, heterozygotes are asymptomatic and show strong protection against malaria (Goheen et al., 2017; Taylor et al., 2012). Likewise, ACKR1 (Duffy antigen, *DARC*) is used by *P. vivax* as a surface receptor for RBC invasion, and the absence of DARC expression partially protects against *P. vivax* infection. In fact, *P. vivax* has driven the fixation of Duffy negativity in sub-Saharan Africa (Culleton et al., 2008; Miller et al., 1976). Deletion of the Cl^-/HCO_3^- anion exchanger of RBCs, SLC4A1, causes southeast Asian ovalocytosis, which is associated with the reduced incidence of malaria (Genton et al., 1995; Jarolim et al., 1991). Furthermore, glucose-6-phosphate dehydrogenase (G6PD) deficiency is high in certain malaria-endemic areas of Africa, Asia, the Middle East, and Papua New Guinea, and has been shown to protect against malaria *in vivo* (Louicharoen et al., 2009). Recently, large genome-wide association studies (GWASs) have confirmed the importance of Hb variants, ABO blood groups, and G6PD in malaria vulnerability, and have also detected novel risk loci *MAVELD3*, *ATP2B4*, glycophorins (*FREM3/GYPE*), and *CD40LG* (Langlais et al., 2017; Band et al., 2015).

The impact of genetic factors on susceptibility to malaria has been investigated in mouse models of CM and SMA caused by infection with *P. berghei* ANKA (*Pb*A) and *P. chabaudi* AS (*Pc*A), respectively. Although neither of these models perfectly reproduce all aspects of pathogenesis of the corresponding human syndromes, they have proven useful for genetic studies, testing drugs, and assessing vaccine candidates (Moradin et al., 2016; Torre et al., 2018). The mouse model of *Pb*A-induced experimental CM (ECM) retains several features of human CM, including brain edema, parenchymal hemorrhage, sequestration of pRBCs, infiltration of inflammatory leukocytes, and severe neurological features that include convulsion, paralysis, and coma (Howland et al., 2015). Likewise, the mouse model of blood-stage malaria induced by *Pc*A shares a number of features with human SMA, including severe anemia, splenomegaly, hepatomegaly with sequestration of infected RBCs in these organs, and stress erythropoiesis (Hernandez-Valladares et al., 2005).

Genes discovered as affecting *Plasmodium* pathogenesis in mice have provided valuable entry points to investigate possible similar effects in human populations (Huang et al., 2018; Torre et al., 2018). We have shown that deficiency in pyruvate kinase (*Pklr*), which is required for glycolysis and ATP synthesis in RBCs, protects mice against blood-stage infection with *Pc*A (reduced blood-stage parasitemia, increased survival) (Min-Oo et al., 2003). Subsequent studies in human RBCs infected *ex vivo* with *P. falciparum* showed that homozygosity or heterozygosity for *PKLR* deficiency reduces infection phenotypes (Ayi et al., 2008). Furthermore, longitudinal studies in populations from malaria-endemic areas showed that heterozygosity for a unique PKLR variant (R41Q) was associated with a reduction in attacks of *P. falciparum* and an increased number of *P. vivax* infections (Berghout et al., 2012; van Bruggen et al., 2015).

In this study, genome-wide chemical mutagenesis was used in mice to identify genes that affect malaria pathogenesis. A mouse mutant that bore a mutation in RBC-specific enzyme bisphosphoglycerate mutase (BPGM) was found to be strongly protected against both blood-stage and cerebral malaria. Our study investigated the mechanism of malaria protection conferred by BPGM deficiency. We observed that at steady state, mutant mice display erythrocytosis (elevated hematocrit [HCT], high Hb) with moderately enhanced erythropoiesis, which is dramatically exacerbated during *Plasmodium* infection. Furthermore, BPGM deficiency is linked to drastic metabolic changes in RBCs, including severely reduced ATP/guanosine triphosphate (GTP) levels, that are associated with impaired parasite maturation and replication. This is concomitant to reduced blood parasitemia levels during *in vivo Plasmodium* infection. Hence, the malaria-protective effect of BPGM deficiency involves metabolic changes in mutant RBCs at steady state and a more robust erythropoiesis in response to decreased oxygen tissue delivery from increased Hb oxygen affinity and also from hemolysis from the parasite replication in pRBCs.

RESULTS

A Mutation in *Bpgm* Protects against ECM Induced by *Pb*A

A genome-wide *in vivo* mutagenesis with *N*-ethyl *N*-nitrosourea (ENU) was used to identify recessively inherited mutations that provide protection against lethal neuroinflammation in a mouse model of ECM induced by *Pb*A (Caignard et al., 2014). Mutagenized B6 G0 males were crossed to wild-type (WT) C57BL/10J (B10) females, and the resulting G1 males were backcrossed to B10 to generate G2 progenies. G2 females were then backcrossed to the G1 male to generate G3 pedigrees, which were phenotyped for resistance to infection with *Pb*A (Figure 1A). While susceptible mice rapidly develop lethal neurological symptoms (tremors, seizures, paralysis, coma) between day 5 (d5) and d8 post-infection (p.i.), ECM-resistant mice remain largely symptom-free and survive beyond d13 p.i.

Several ECM-resistant mice appeared in pedigrees from the G1 male Darrion. Exome sequencing of 3 resistant G3 mice identified a homozygous mutation in exon 2 of the *Bpgm* gene (T-to-C nucleotide transversion), causing a non-conservative leucine-to-proline substitution at position 166 (L166P; $Bpgm^{L166P}$) (Figure 1B). $Bpgm^{L166P}$ homozygotes were partially but significantly protected against ECM, with survival beyond d10 in >50% of mice, compared to heterozygotes ($Bpgm^{L166P/+}$) and WT B6, which were ECM susceptible (Figure 1C). Loss of integrity of the blood-brain barrier (BBB) is a pathological feature of lethal neuroinflammation in ECM-susceptible animals that can be assessed by Evans blue extravasation (Figures 1D and 1E; Ghazanfari et al., 2018). In contrast to *Pb*A-infected B6 controls who readily accumulated the dye (at d6 p.i.), $Bpgm^{L166P}$ mice showed reduced dye accumulation, indicating the retention of BBB integrity. Another feature of *Pb*A-induced ECM is the infiltration of inflammatory myeloid and lymphoid cells in the brain that drives pathogenesis in susceptible animals. Investigation of cellular infiltration in the brain of *Pb*A-infected mice at d6 p.i. by flow cytometry (fluorescence-activated cell sorting [FACS]) showed significantly reduced accumulation of $CD45^+$ cells in ECM-resistant $Bpgm^{L166P}$ mice, compared to controls, including decreased numbers of $CD4^+$ and $CD8^+$ T cells, B cells, macrophages,

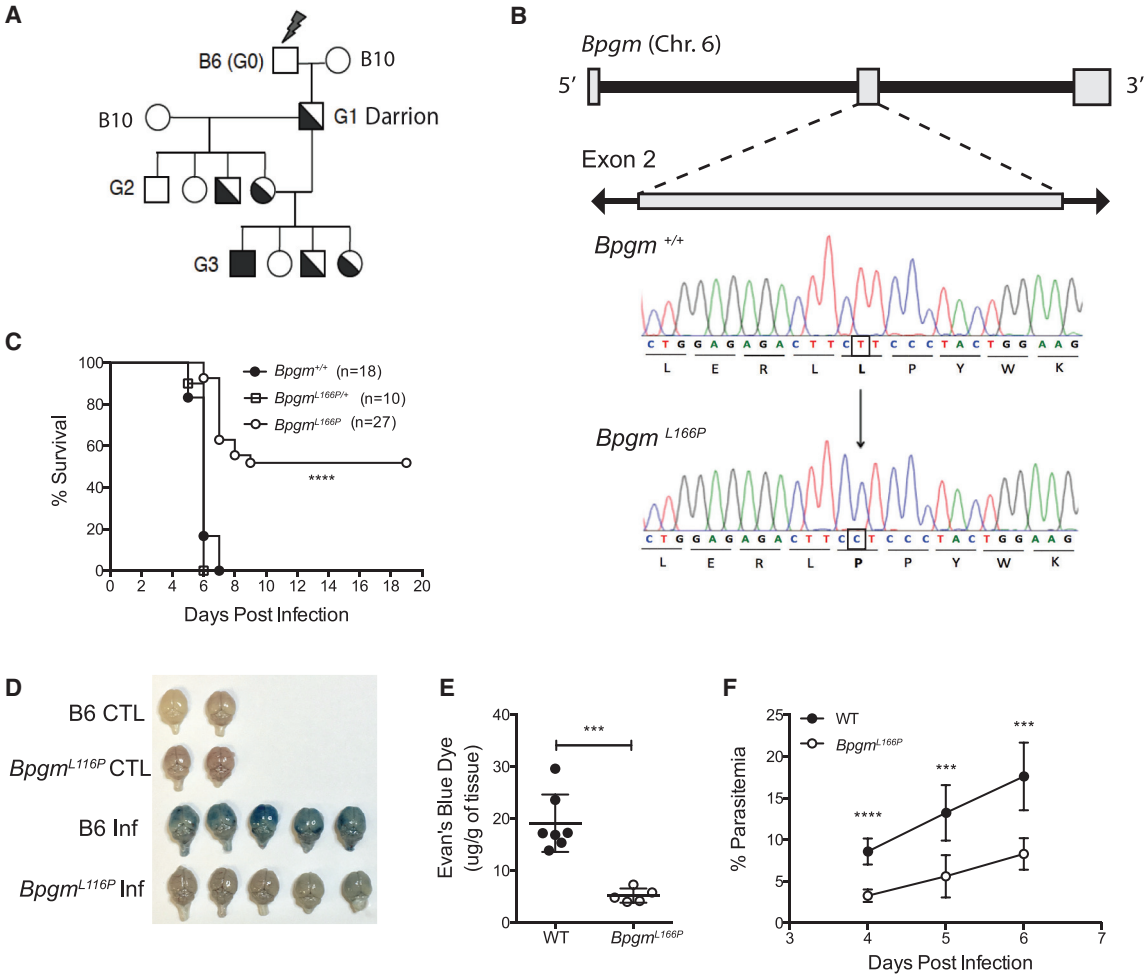

Figure 1. An ENU-Induced Mutation in *Bpgm* Protects against ECM Induced by *Pb*A

(A) Breeding scheme for the production of ENU-induced homozygote mutants. G2 females were backcrossed to the G1 male (Darrion) to generate G3 offspring that were phenotyped for susceptibility to *Pb*A-induced ECM.

(B) Whole-exome sequencing identified a L166P amino acid substitution in exon 2 of *Bpgm* in mice derived from the Darrion pedigree.

(C) Male and female mice were infected with *Pb*A; survival of WT ($Bpgm^{+/+}$; n = 18), heterozygote ($Bpgm^{L166P/+}$; n = 10), and homozygote mutants ($Bpgm^{L166P}$; n = 27) are shown. A log-rank (Mantel-Cox) test was used to determine significance (****p < 0.0001).

(D) Evans blue dye extravasation assay was performed to assess the integrity of the BBB. WT and $Bpgm^{L166P}$ mice were injected with Evans blue dye on d6 p.i. with *Pb*A, and brains were dissected and photographed.

(E) The dye was extracted from the brain 1 h post-injection and quantified by optical density measured at 610 nm, and expressed as micrograms of dye per gram of tissue.

(F) Blood-stage parasitemia levels were determined on thin blood smears and are expressed as a fraction of pRBC (% parasitemia). A minimum of 500 RBCs were counted per mouse.

The data in (E) and (F) are presented as means ± SDs; p values are calculated using 2-tailed unpaired Student's t test (***p < 0.001; ****p < 0.0001). See also Figure S1.

and neutrophils (Figure S1). Blood parasitemia (percentage of pRBCs) levels tested at days 4, 5, and 6 p.i. (Figure 1F) were significantly lower in $Bpgm^{L166P}$ mice than in controls (total parasite load 0.779 × 10^9 ± 0.047 versus 1.268 × 10^9 ± 0.067/mL of blood, respectively; p < 0.0005), suggesting a primary effect of the mutation on parasite replication in blood. These results show that ECM resistance in $Bpgm^{L166P}$ mutants is expressed primarily as reduced blood-stage replication of the parasite concomitant to decreased intensity of neuroinflammation.

L166P Impairs BPGM Protein Stability and Function in RBC

BPGM is an RBC-specific trifunctional enzyme that synthesizes 2,3-bisphosphoglycerate (2,3-BPG). This enzyme bypasses the generation of 1 molecule of ATP in glycolysis (the Rapoport-Luebering shunt), which in turn generates an important glycolytic intermediate, 2,3-BPG, that facilitates Hb oxygen delivery (Chu et al., 2014; van Wijk and van Solinge, 2005). From BPGM solved structure, L166P does not map to any known functional domains involved in the BPGM catalytic cycle (Craescu et al., 1992;

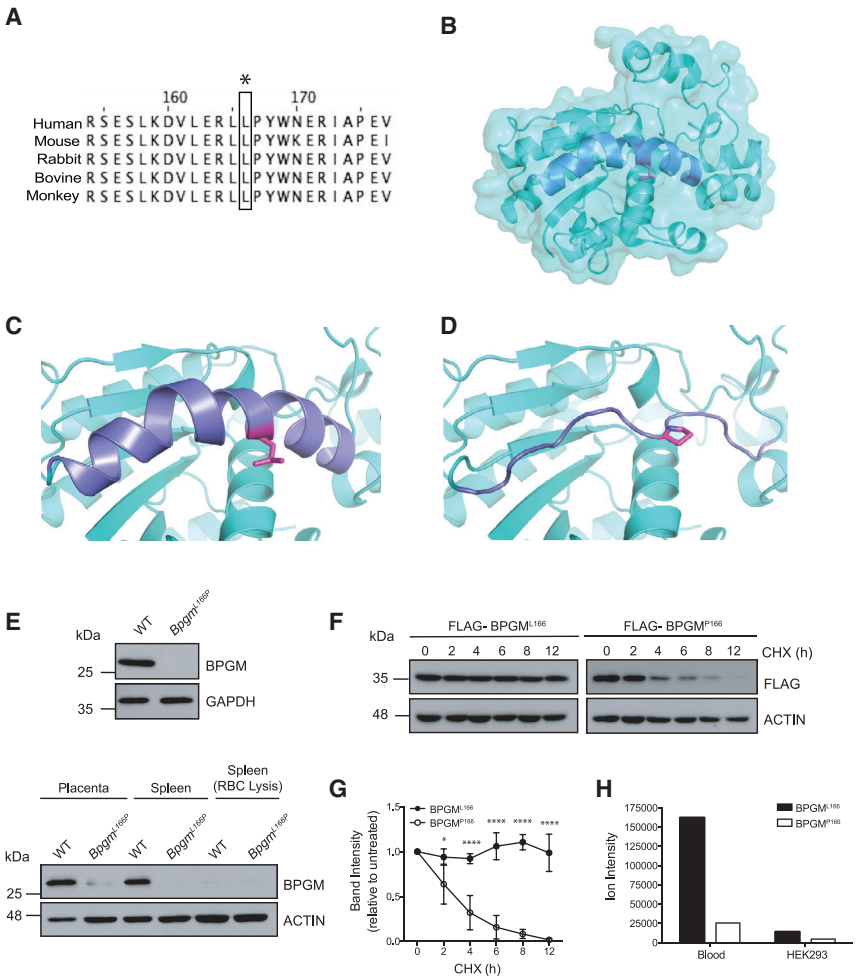

Figure 2. Leucine-to-Proline Substitution at Position 166 Impairs BPGM Stability and Activity

(A) Multiple sequence alignment of BPGM shows that leucine at position 166 is invariant across vertebrates.

(B) Surface diagram of WT BPGM (cyan). Residue L166 (magenta), depicted in stick representation, is located in helix 7 (purple).

(C) Close-up of WT BPGM focusing on residue L166.

(D) Close-up of P166 BPGM variant featuring the unraveling of helix 7, with P166 mutation (magenta) depicted in stick representation.

(E) Protein extracts from whole blood (top panel), placenta, spleen, and splenocytes (after RBC lysis; bottom panel) of WT and *Bpgm*^{L166P} mice were analyzed for BPGM protein expression by immunoblotting. The expected molecular mass of BPGM is 30kDa.

(F) Stability of WT (BPGM^{L166}) and mutant (BPGM^{P166}) variants expressed in transfected HEK293 cells as FLAG-tagged recombinant proteins were analyzed by immunoblotting following treatment with CHX (100 μg/mL) for 2, 4, 6, 8, and 12 h.

(G) BPGM immunoreactive bands from (F) were quantified by ImageJ (NIH), normalized to the actin control, and expressed as a fraction of signal in untreated sample (T = 0 h). The data are shown as means ± SDs; p values are calculated using Sidak's multiple comparison tests (*p < 0.05; ****p < 0.0001) for 3 independent experiments.

(H) LC-MS analysis of 2,3-BPG levels in the blood of WT and *Bpgm*^{L166P} mice, and transfected HEK293 cells expressing BPGM^{L166} or the BPGM^{P166} variant.

Patterson et al., 2010; Wang et al., 2004). However, L166 is invariant among vertebrates, and the L166P substitution is non-conservative, suggesting possible structural or functional effects on BPGM (Figure 2A). Furthermore, molecular modeling of L166P on the structure of BPGM predicts that P166 causes a major structural change, including the loss of a domain-linking α-helix (Figures 2B–2D; Kundu et al., 2013).

BPGM is a 30-kDa protein that is known to be highly expressed in erythroid cells and RBC-rich organs (Pritlove et al., 2006). Comparative protein expression shows abundant BPGM expression in the RBCs, spleen, and placenta of controls, while in some of the *Bpgm*^{L166P} mutants, the protein is undetectable (Figure 2E), suggesting that L166P adversely affects protein expression or stability in primary cells. This was further investigated in HEK293 cells stably expressing transfected epitope-tagged (FLAG) WT (L166) and mutant (P166) BPGM, and was treated with the protein synthesis inhibitor cycloheximide (CHX). The disappearance of BPGM was monitored over time by immunoblotting (Figure 2F) and was quantified (Figure 2G). While the half-life of WT L166 variant was measured at >10 h, the half-life of mutant P166 variant was reduced to <3 h (Figures 2F and 2G). Finally, the amount of 2,3-BPG in primary RBCs from WT and *Bpgm*^{L166P} mutants and in HEK293 cells stably expressing transfected L166 and P166 proteins was determined (Figure 2H). There was a strong reduction in 2,3-BPG levels in mutant RBCs and in corresponding transfected cells compared to controls. These results suggest a loss of stability of the P166 variant linked to a possible misfolding of the protein that ultimately leads to a loss of enzymatic activity in the erythroid cells.

Bpgm^{L166P} Mutants Display Erythrocytosis

We assessed the effect of *Bpgm*^{L166P} on hematological parameters at steady state (Figure 3A). Compared to WT controls, *Bpgm*^{L166P} mutants exhibited increased HCT (95% confidence interval [CI], 0.05054–0.09126 L/L, $p < 0.001$), RBC (95% CI, 0.3470–1.189 × 10^{12}/L, $p < 0.01$), Hb (95% CI, 9.617–24.78 L/L, $p < 0.001$), and mean corpuscular Hb (MCH) (95% CI, 0.02792–0.9121 pg, $p < 0.5$) levels and developed significant macrocytosis of their RBCs, concomitant with elevated serum erythropoietin (EPO) levels (Figure 3B). There was no effect of the *Bpgm*^{L166P} mutation on the percentage of circulating reticulocytes and no

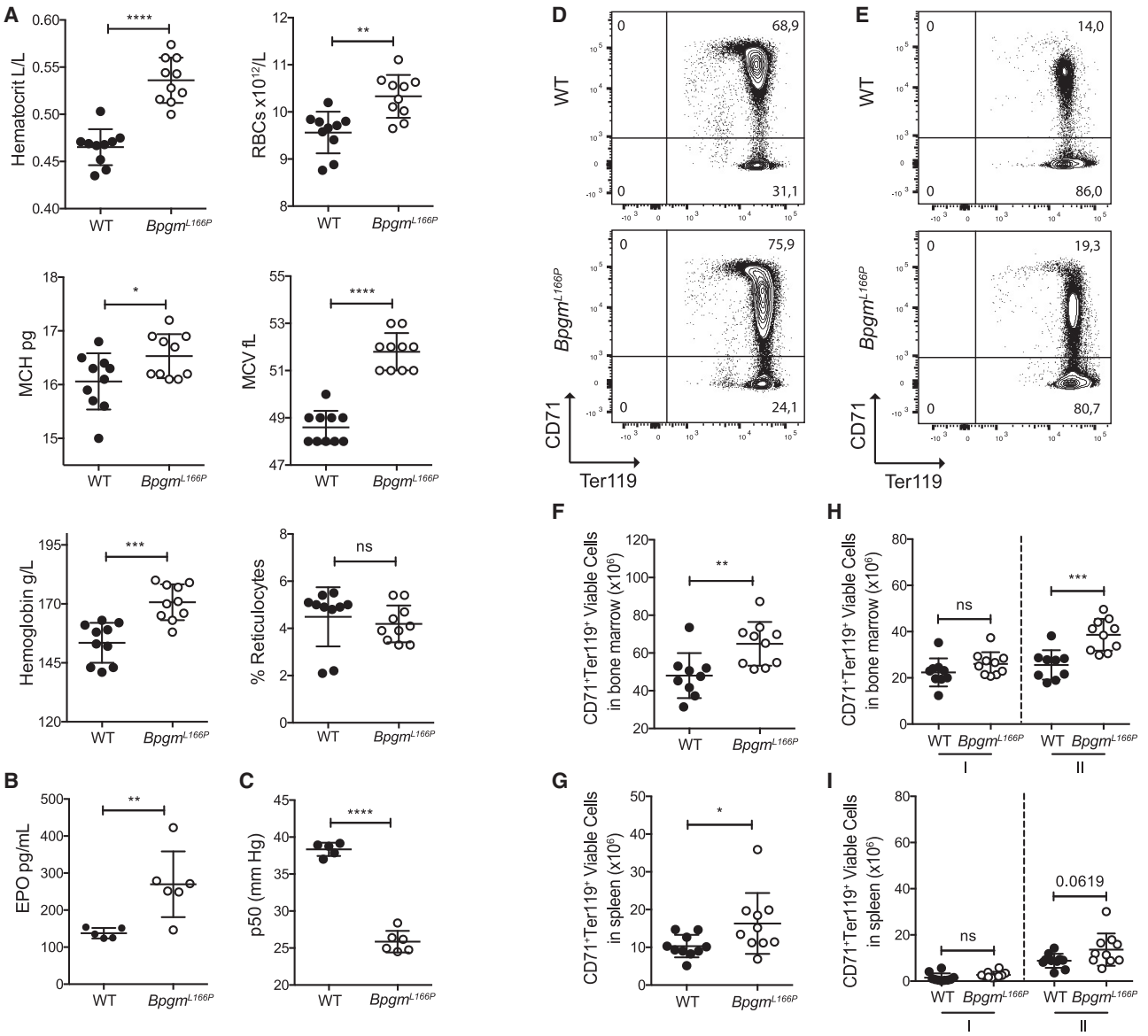

Figure 3. *Bpgm*^{L166P} Mutant Mice Display Erythroid Abnormalities at Steady State

(A and B) Hematological parameters of WT or *Bpgm*^{L166P} mutants were assessed (n = 10 per group) (A), along with serum EPO levels (B). MCH, mean corpuscular hemoglobin; MCV, mean corpuscular volume; RBC, red blood cells.

(C) p50 values calculated from venous blood analysis from WT (n = 5) and *Bpgm*^{L166P} mutants (n = 6).

(D and E) Bone marrow (D) and splenic (E) cells from WT and *Bpgm*^{L166P} mice were labeled with antibodies against erythroid markers CD71 and Ter119 (CD71$^+$/Ter119$^+$ total erythroid precursors) and analyzed by flow cytometry (FACS) at steady state. Representative FACS contour plots are shown, with the proportion of total cells in quadrant indicated by number.

(F and G) CD71$^+$Ter119$^+$ viable cells in the bone marrow (F) and spleen (G) are shown.

(H and I) CD71 and FSC-H were used to further identify sub-populations of CD71$^+$Ter119$^+$ erythroid precursors into group I (erythroblast populations: pro-erythroblasts, basophilic, polychromatophilic, and orthochromatophilic erythroblasts) and group II (reticulocytes) (gating strategy shown in Figure S2). Each dot represents 1 mouse.

All of the data are shown as means ± SDs. Statistical significance was calculated using 2-tailed unpaired Student's t test (*p < 0.05; **p < 0.001; ***p < 0.001; ****p < 0.0001; ns, non-significant). See also Figures S2–S4.

associated splenomegaly (data not shown). These findings suggest that *Bpgm*^{L166P} loss-of-function mutation causes erythrocytosis, which is similar to clinical reports of BPGM-deficient patients (Lemarchandel et al., 1992; Petousi et al., 2014).

In humans, erythrocytosis in rarely reported patients with 2,3-BPG deficiency is associated with the increased affinity of Hb for oxygen and the decreased rate of oxyhemoglobin dissociation (Prchal and Gregg, 2005). The Hb oxygen dissociation curve is

the relationship between the oxygen tension and the Hb oxygen saturation in blood, with p50 being the oxygen tension when Hb is 50% saturated with oxygen. When Hb-oxygen affinity increases, the oxyhemoglobin dissociation curve shifts to the left and decreases p50 and thus tissue oxygen delivery. Since in venous blood, where Hb oxygen is markedly decreased compared to arterial blood, one can determine the p50 values from venous blood using its pH, pO_2, and Hb oxygen saturation (Agarwal et al., 2007; Lichtman et al., 1976). When this was performed in WT and *Bpgm*^{L166P} mutant mice (Figure 3C), the *Bpgm*^{L166P} mutation was found to be associated with significantly decreased p50 in mutant (26 mmHg) versus controls (36 mmHg), reflecting increased intrinsic affinity of Hb for oxygen in the mutant (left-shifted Hb oxygen dissociation).

The effect of *Bpgm*^{L166P} on erythropoiesis in bone marrow and spleen was monitored at steady state using the expression of the transferrin receptor (CD71) and glycophorin A-associated protein (Ter119) and published flow cytometry (FACS) gating strategies (Figure S2A; Chen et al., 2009; Koulnis et al., 2011; Liu et al., 2006). An increase in the percentage and total numbers of CD71$^+$Ter119$^+$ cells was detected in the bone marrow and spleen of mutants compared to controls (Figures 3D–3G). Sub-populations of erythroid progenitors can be further distinguished by forward scatter intensity (FSC) to estimate cell size (Chen et al., 2009; Liu et al., 2006), segregating group I erythroblasts, which represent all of the stages of maturing erythroblasts, and group II, which represents reticulocytes. Compared to controls, the total number of CD71$^+$Ter119$^+$ reticulocytes in *Bpgm*^{L166P} mice showed a marked significant increase in the bone marrow (95% CI, 6.603–19.48 × 10^6 cells, $p < 0.001$) (Figure 3H), with a similar trend noted in the spleen (95% CI, −0.2664 to 9.874 × 10^6 cells, $p = 0.0619$) (Figure 3I). Moreover, erythroid precursors from *Bpgm*^{L166P} mutants in the bone marrow and spleen displayed a significant decrease (median fluorescence intensity [MFI]) in CD71 expression (Figures S2B–S2E). Further immunophenotyping by FACS using cell-specific markers failed to detect a major effect of the *Bpgm*^{L166P} mutation on major immunocyte compartments in the spleen and bone marrow (Figures S3 and S4).

These results indicate that the *Bpgm*^{L166P} mutation is associated with the increased intrinsic affinity of Hb for oxygen and the increased erythropoiesis in the bone marrow and spleen at steady state.

Increased Stress Erythropoiesis Response to *Plasmodium* Infection in *Bpgm*^{L166P} Mutants

The impact of the *Bpgm*^{L166P} mutation on erythroid response to malaria was first tested in the *Pb*A model of ECM by monitoring erythroid populations on d6 p.i., before the onset of mortality in WT controls (Figure 4). *Bpgm*^{L166P} mutants reflected increased erythropoietic activity in the periphery with a higher percentage of circulating reticulocytes (Figure 4A), concomitant with significant splenomegaly (Figures 4B and 4C). In response to *Pb*A infection, both controls and mutants showed a marked increase in erythropoiesis; however, this response was higher in the mutant, with greater numbers and proportion of CD71$^+$Ter119$^+$ erythroid precursors in the bone marrow (Figures 4D and 4F) and spleen (Figures 4E and 4G). The stronger response of *Bpgm*^{L166P} mutants was seen for both group I and group II precursors (Figures 4H and 4I). This increased erythropoietic response may contribute to a faster recovery from hemolytic stress induced by *Pb*A infection, hence dampening disease severity in the mutant (Fowkes et al., 2008; Lamikanra et al., 2007).

An erythroid mechanism of protection against *Pb*A-induced ECM would be a unique situation since ECM-resistant mutants previously identified in our screen invariably involved mutations dampening neuroinflammation, with no impact on blood-stage parasitemia (Bongfen et al., 2012; Kennedy et al., 2014; Torre et al., 2015, 2017). Hence, we tested the impact of *Bpgm*^{L166P} in response to infection with *Pc*A, a parasite whose pathogenesis is strictly restricted to blood-stage replication, with high levels of parasitemia causing lethal anemia, without CM (Chang and Stevenson, 2004). Inbred mouse strains have different susceptibilities to *Pc*A-induced blood-stage malaria, with B6 mice (onto which the *Bpgm*^{L166P} mutation arose) being highly resistant (Stevenson et al., 1982; Yap and Stevenson, 1992). To test a protective effect of *Bpgm*^{L166P} against blood-stage disease, we backcrossed the *Bpgm*^{L166P} mutant allele on the *Pc*A-susceptible genetic background of A/J mice (A/J.*Bpgm*^{L166P} strain). The transfer of the *Bpgm*^{L166P} mutation onto the A/J background protected A/J.*Bpgm*^{L166P} mice against blood-stage infection, with increased survival (Figure 5A; 80% survival), with reduced blood parasitemia throughout (Figure 5B), and at the peak of infection (Figure 5C; 44% peak parasitemia), when compared to A/J controls (100% lethality; 58% peak parasitemia). In addition, A/J.*Bpgm*^{L166P} mice contained the infection, exhibiting a progressive decrease in parasitemia starting at d10 and continuing up to d20 p.i. (Figure 5B). These results show that A/J.*Bpgm*^{L166P} mice can restrict the blood-stage replication of *Pc*A and show a greater capacity to recover from high parasitemia, demonstrating a strong protective effect of BPGM deficiency against severe malaria-induced anemia.

The effect of the *Bpgm*^{L166P} mutation on the erythropoietic response during induction and recovery from *Pc*A-induced hemolytic stress was also investigated. To corroborate the results of these experiments with those obtained in *Pb*A infection (Figures 1, 3, and 4), we used the original *Bpgm*^{L166P} stock on a B6 genetic background, which, albeit resistant to *Pc*A infection, is still informative for the effect of the *Bpgm* mutation on erythroid parameters. On d10 p.i., *Bpgm*^{L166P} mutants exhibited splenomegaly (Figures 5D and 5E), accompanied by an ~2-fold increased expansion of CD71$^+$Ter119$^+$ erythroid cells of the spleen (groups I and II), in comparison to WT controls (Figures 5F and 5G). No significant differences were observed in the number of CD71$^+$Ter119$^+$ erythroid precursors between *Bpgm*^{L166P} and WT mice in the bone marrow at that time point (Figures S5A and S5B). These results suggest a more robust erythroid response in *Bpgm*^{L166P} mutants compared to controls following a purely hemolytic infection with *Pc*A. Our data are in agreement with the reported critical importance of splenic stress erythropoiesis to the outcome of malaria (Weiss et al., 1989; Yap and Stevenson, 1992). The results demonstrate that the *Bpgm*^{L166P} mutation confers protection against both blood stage and CM in mouse models of these diseases, linked in part to the superior erythroid response of the mutant.

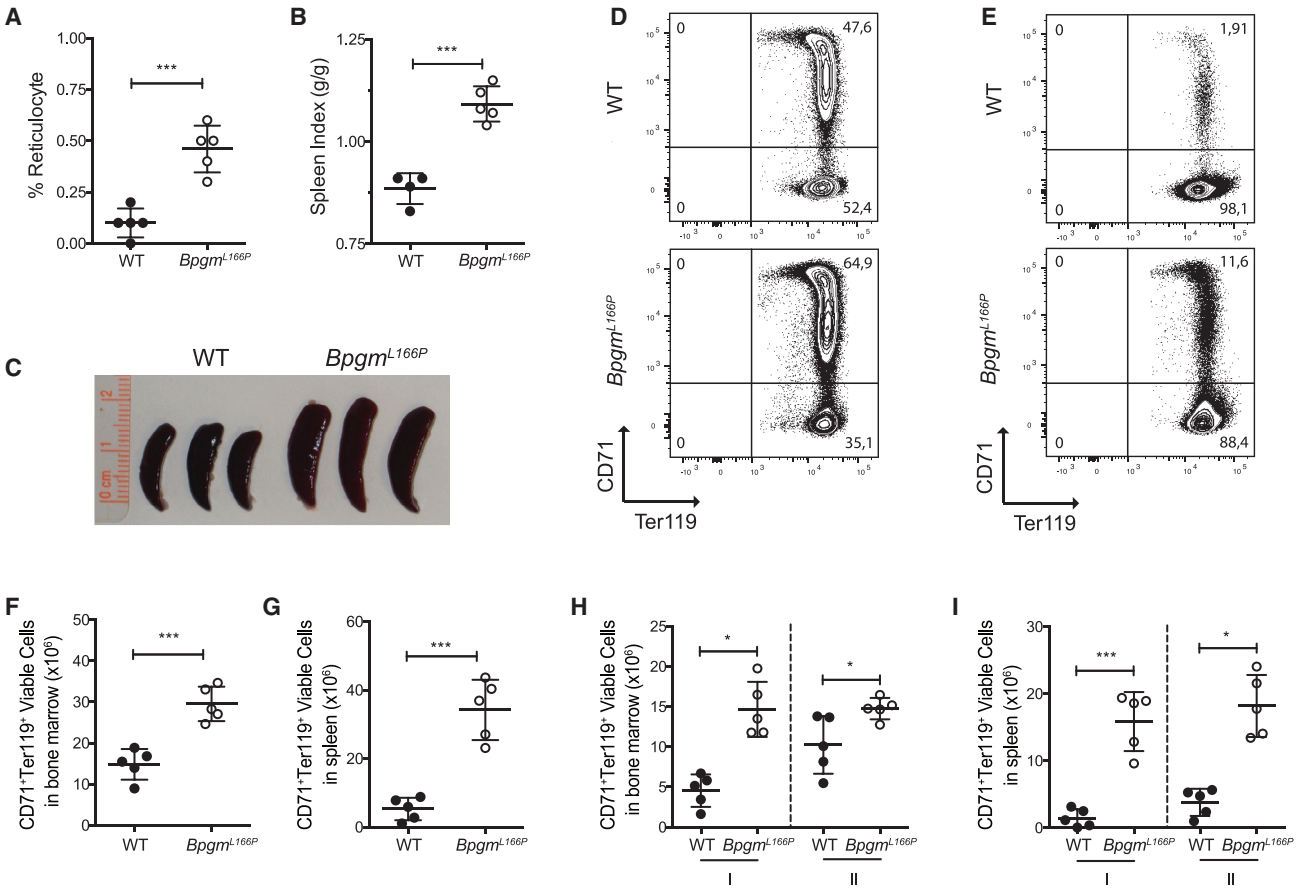

Figure 4. Altered Erythropoietic Response of *Bpgm*^{L166P} Mutants in Response to *Pb*A-Induced ECM

Erythroid response of WT and *Bpgm*^{L166P} mice to *Pb*A infection (d6 p.i.).

(A) Reticulocytes were counted on thin blood smears stained with new methylene blue (1,000 cells per data point) and expressed as a percentage of total RBCs.

(B) Spleen index was calculated as the square root of the mass of the spleen (grams) divided by the body mass (grams).

(C) Photographs of infected spleens from WT and *Bpgm*^{L166P} mutants (d6 p.i.).

(D–G) FACS analysis of CD71^{+}Ter119^{+} cells from the bone marrow (D) and spleen (E) of *Pb*A-infected control and mutant mice. Representative contour plots are shown in (D) and (E), while total numbers are shown in (F) and (G), respectively.

(H and I) Similar to Figure 3, CD71 and FSC-H were used to distinguish the subpopulations of erythroid progenitors (I, erythroblast populations; II, reticulocytes), demonstrating a greater number of these cells in *Pb*A-infected mutant mice compared to controls. Each dot represents 1 mouse.

All of the data are shown as means ± SDs. Statistical significance was calculated using 2-tailed unpaired Student's t test (*$p < 0.05$; ***$p < 0.001$).

Finally, we tested the erythroid response of the mutant to hemolytic anemia caused by phenylhydrazine (PHZ; Figures 5H, 5I, S5C, and S5D). Compared to controls, *Bpgm*^{L166P} mutants showed elevated erythropoietic activity in the spleen in the form of increased group I and II of CD71^{+}Ter119^{+} erythroid precursors (Figures 5H and 5I). These observations suggest a stronger erythropoietic response of *Bpgm*^{L166P} mutants, irrespective of the nature of the hemolytic stimulus.

Reduced Intra-erythrocytic Replication of *Plasmodium* in *Bpgm*^{L166P} Mutant Cells *In Vivo*

We monitored the capacity of *Pb*A and *Pc*A parasites to replicate in RBCs from control and *Bpgm*^{L166P} mutants. *Plasmodium* development in RBC infected *in vivo* was analyzed by monitoring parasite DNA (Hoechst stain) in cells by FACS, using a CD71/Ter119 gating strategy (Figure S6; Malleret et al., 2011, 2015). This DNA staining procedure can also estimate the numbers and frequency of ring forms versus late-stage forms to monitor both replication and maturation of intra-erythrocytic parasites (Figure S6). We observed an ~5% decrease in the proportion of *Plasmodium* late-stage parasites in mutant RBCs compared to controls for both *Pb*A infection (95% CI, −6.560 to −1.756, $p < 0.01$) (Figures 6A–6C) and *Pc*A infection (95% CI, −12.07 to −1.013, $p < 0.05$) (Figures 6D–6F). This suggests that the *Bpgm*^{L166P} mutation creates an intracellular environment that is less permissive to replication and maturation of the malarial parasite in RBCs.

Effect of the *Bpgm*^{L166P} Mutation on RBC Metabolism

Steady-state metabolites levels were analyzed in WT and mutant RBC extracts (Method Details) with relative quantitation of 134 detected metabolites (Table S1). MetaboAnalyst 3.0 (Xia et al.,

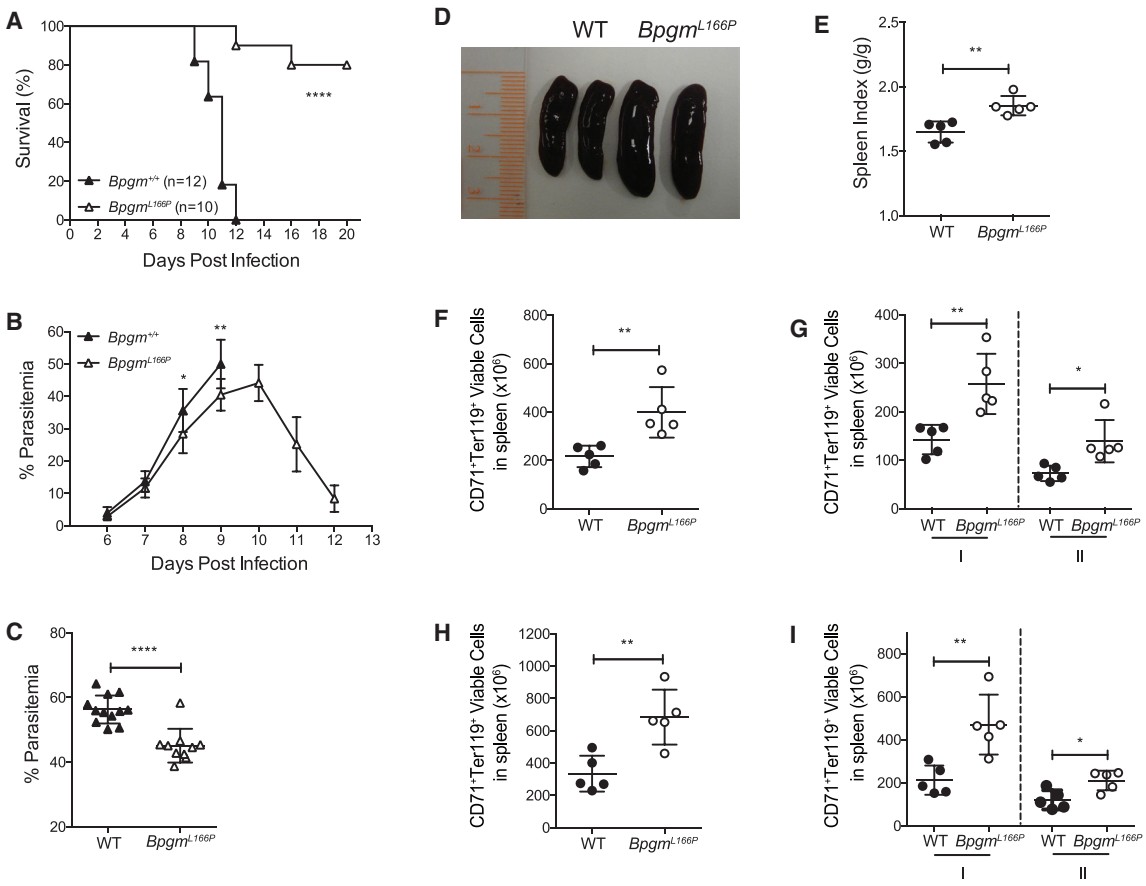

Figure 5. Altered Erythropoietic Response of *Bpgm*^{L166P} Mutants following *Pc*A-Induced Blood-Stage Malaria

Bpgm^{L166P} was introduced in the genetic background of *Pc*A-susceptible A/J mice (A/J.*Bpgm*^{L166P}). Control (A/J) and mutant mice (A/J.*Bpgm*^{L166P}) were infected with *Pc*A.

(A) Survival plot of infected WT female and A/J.*Bpgm*^{L166P} female mutant mice. A log-rank (Mantel-Cox) test was used to calculate significance (****$p < 0.0001$).

(B) Blood parasitemia levels were determined on thin blood smears and were plotted over the period of time that preceded mortality in A/J controls.

(C) Maximum blood-stage replication during this period is shown and expressed as the peak parasitemia. A minimum of 500 RBCs were counted per data point shown. The effect of *Bpgm*^{L166P} mutation on erythropoietic response was analyzed on d10 p.i. of WT and *Bpgm*^{L166P} mutants (on a resistant B6 background) with *Pc*A.

(D and E) Representative spleens of WT and *Bpgm*^{L166P} mice identified splenomegaly in mutant mice (D), which was quantified in (E).

(F) Significant increase in CD71^{+}Ter119^{+} maturing erythroid precursors in the spleen of *Pc*A-infected *Bpgm*^{L166P} mice.

(G) Significant increase in group I and group II CD71^{+}Ter119^{+} maturing erythroid precursors in the spleens of *Pc*A-infected *Bpgm*^{L166P} mice compared to controls.

(H and I) WT and *Bpgm*^{L166P} mice were treated with PHZ at 50 mg/kg body weight on d0. Erythroid cell populations were analyzed on d5 post-injection. Similar analysis to (F) and (G), but for CD71^{+}Ter119^{+} maturing erythroid precursors in the spleen following treatment with PHZ.

All of the data are shown as means ± SDs, with the exception of (A). Statistical significance was calculated using 2-tailed unpaired Student's t test (*$p < 0.05$; **$p < 0.001$; ****$p < 0.0001$).

2015), unsupervised principal-component analysis (PCA), and partial least-squares discriminant analysis (PLS-DA) were used to generate two-dimensional score plots (Figure 7A). Hierarchical clustering analysis of the top differentially present 50 metabolites is shown in Figure 7B as a heatmap, in Figure 7C as a volcano plot (adjusted $p < 0.05$ and a fold change [FC] ≥ 1.5), and in Table S2. Overall, the *Bpgm*^{L166P} mutation strongly affects several metabolites and associated pathways. As expected and relative to WT cells, *Bpgm*^{L166P} RBCs show the accumulation of 1,3-BPG and the almost complete absence of 2,3-BPG in agreement with the loss of BPGM enzymatic function (Figure 7C). The *Bpgm*^{L166P} mutation is associated with a strong reduction of all triphosphate, diphosphate, and monophosphate nucleotide pools (ATP, GTP, UTP, TTP) compared to controls, suggesting that purine/pyrimidine energy metabolism is compromised in mutant RBCs (Figure 7D). Reduced ATP levels have been associated with decreased permissiveness of *Plasmodium* replication in mouse and human models of PKLR deficiency (Ayi et al., 2009; Min-Oo et al., 2003). Metabolite set enrichment analysis identified significant enrichment ($p \leq 0.05$) for other differentially expressed metabolites and pathways, including amino acid metabolism, and pentose phosphate pathway, suggesting further pleiotropic effects of the mutation (Figures S7A and S7B).

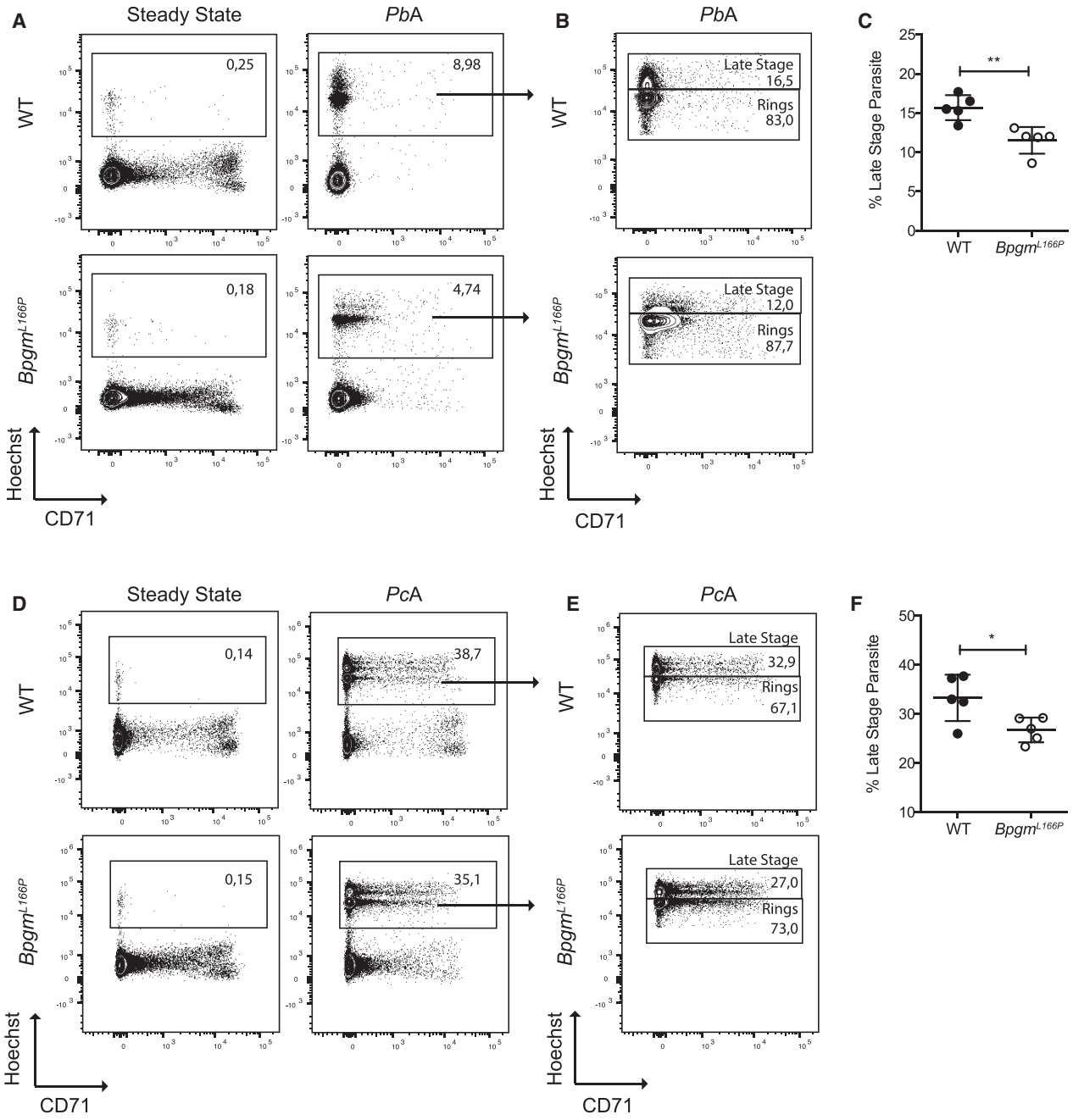

Figure 6. *Bpgm*^{L166P} Impairs Intraerythrocytic Growth of *Plasmodium* Parasites

FACS analysis was performed on whole blood from *Pb*A- and *Pc*A-infected WT and *Bpgm*^{L166P} mutant mice using a method adapted from Malleret et al. (2011, 2015) (see Figure S6). Mice were infected with either 10^6 *Pb*A-pRBC or 10^5 *Pc*A-pRBC intravenously.

On d6 p.i. with *Pb*A (A–C) or d7 p.i. with *Pc*A (D–F), blood was stained with Hoechst 33342 and with anti-CD71 and anti-Ter119 antibodies.

(A and D) The proportion of total pRBC is defined as Hoechst positive cells, and are indicated.

(B and E) Cells displaying lower or higher Hoechst signals contain ring-stage parasites and late-stage parasites, respectively.

(C and F) The proportion of intracellular late-stage *Pb*A and *Pc*A parasites are graphed for WT controls and for *Bpgm*^{L166P} mutant-infected RBCs, showing a significant decrease in the proportion of late-stage parasites in the mutant.

All of the data are shown as means ± SDs. A 2-tailed unpaired Student's t test was used to calculate significance (*$p < 0.05$; **$p < 0.001$). Related to Figure S6.

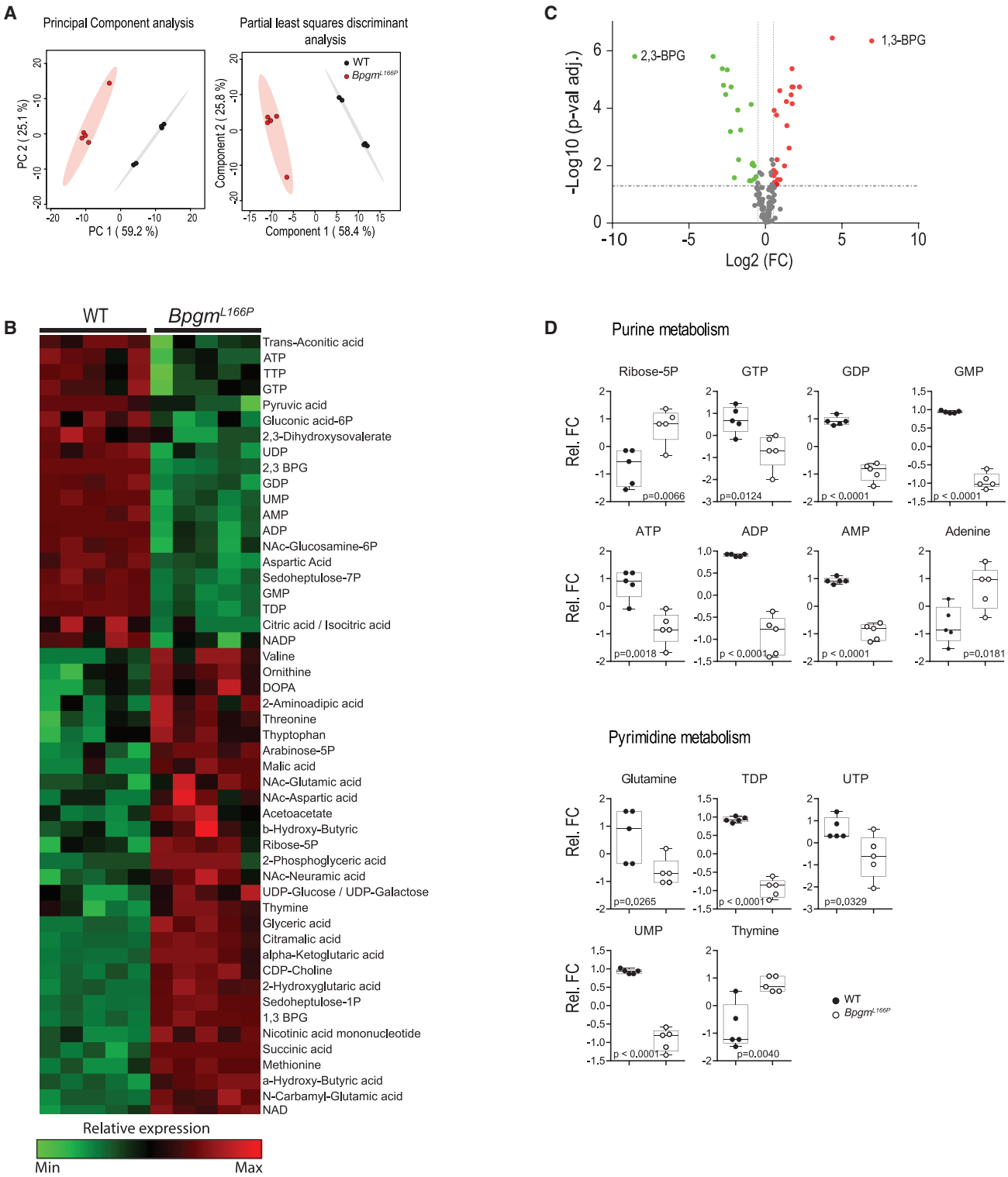

Figure 7. BPGM Deficiency Affects RBC Metabolic Pathways

(A) PCA and PLS-DA from the metabolic profiles of normalized (median normalized and log-transformed) and background-corrected values of WT (n = 5) and *Bpgm*^{L166P} (n = 5) mice RBC replicates. Each point represents an extract from an individual mouse.

(legend continued on next page)

These results indicate that BPGM deficiency has a strong effect on the intracellular milieu of RBCs, including decreased energy metabolism with very low ATP/GTP pools.

DISCUSSION

We have identified a novel ENU-induced mutation that protects mice *in vivo* against lethal cerebral malaria (*Pb*A). ECM protection in these mice is phenotypically expressed as reduced severe anemia and blood parasitemia, absence of neurological symptoms, and increased survival. As opposed to previous protective mutations identified in our screen (*Themis*, *Jak3*, *Usp15*, *Ccdc88b, Irf8, Irf1*) that cause imbalance in inflammatory responses to infection, this mutation does not seem to affect the number or function of immune cells (Torre et al., 2018). Instead, the mutation affects RBC protein BPGM ($Bpgm^{L166P}$). In addition, the mutation protects against blood-stage malaria (*Pc*A), with protection similarly expressed as reduced parasitemia and increased survival. The combined protective effect of the $Bpgm^{L166P}$ mutation against different *Plasmodium* parasites that cause lethality by distinct pathologies (ECM versus SMA), but yet use the RBC as a replicative niche, first suggested a non-immune, RBC-specific effect of $Bpgm^{L166P}$ that would impede parasite replication, causing reduced blood-stage parasitemia and ultimately reduced lethality in both ECM (*Pb*A) and SMA (*Pc*A) models.

BPGM is an RBC-specific enzyme that synthesizes 2,3-BPG from 1,3-BPG (Chu et al., 2014). The L166P variant causes loss of BPGM function in mutant RBCs: (1) it affects a highly conserved residue (L166) in the protein; (2) the leucine-to-proline substitution at position 166 is predicted to affect BPGM structure, including loss of a structured α-helix; (3) the P166 variant is unstable with a reduced half-life, and is virtually undetectable in mutant mature RBCs; and (d) RBCs from $Bpgm^{L166P}$ mice or transfected cells expressing the L166P variant show severely reduced 2,3-BPG levels. In RBCs, 2,3-BPG is the main allosteric regulator of Hb. 2,3-BPG shifts the equilibrium between the oxy and deoxy states of Hb by preferentially stabilizing the unliganded form (Hong and Gotlib, 2014; van Wijk and van Solinge, 2005). BPGM deficiency in $Bpgm^{L166P}$ mutants causes erythrocytosis, with elevated circulating RBCs and total Hb, and increased erythropoiesis ($Ter119^{+}/CD71^{+}$ erythroid precursors) in the bone marrow and spleen at steady state. This is attributed to insufficient levels of 2,3-BPG, resulting in increased O_2-bound Hb, decreased oxygen delivery to tissues (lower p50), and compensatory erythropoiesis (Hoyer et al., 2004; Oliveira et al., 2018). Our studies show that the $Bpgm^{L166P}$ mutant identified in our screen phenotypically mimics human BPGM deficiency with the accumulation of 1,3-BPG and an almost complete absence of 2,3-BPG , reduced rate of oxygen dissociation from Hb, and decrease in corresponding p50 values.

We propose that BPGM deficiency protects against malaria through a dual mechanism that involves (1) a more productive erythropoietic response to replenish the loss of *Plasmodium*-infected RBCs and (2) a reduced rate of intraerythrocytic parasite replication in mutant RBCs. The loss of BPGM is associated with an increased erythropoiesis at steady state linked to the reduced gaseous exchange performance of mutant RBCs. However, in response to hemolytic stress caused by infection with either *Pb*A and *Pc*A (or following treatment with PHZ), compensatory stress erythropoiesis is dramatically superior in mutant mice compared to controls, particularly in the spleen. Superior erythropoiesis response to mounting parasitemia and RBC destruction is expected to provide a significant physiological advantage via more efficient replacement of infected RBCs. This would dampen the malaria-induced anemia and would allow other protective physiological responses to develop (immune functions). In humans and in mouse models of experimental infection, the strength of the erythroid response is a key determinant of the severity of blood-stage disease. Low reticulocytosis is a major factor in the onset and intensity of SMA, while recovery is compromised by inadequate erythropoiesis (Chang and Stevenson, 2004; Lamikanra et al., 2007; White, 2018). Also, in humans, dys-erythropoiesis in the bone marrow has been found in *P. falciparum*- and *P. vivax*-infected individuals, while in mouse models, protection against SMA is linked to the dramatic amplification of splenic erythropoiesis (Abdalla et al., 1980; Chang and Stevenson, 2004; Weiss et al., 1989; Wickramasinghe et al., 1989). These observations support superior erythropoiesis as contributing to the malaria-protective effect of BPGM deficiency.

A second mechanism by which BPGM deficiency may contribute to malaria protection (and reduced blood-stage parasitemia) is through reduced intracellular replication of the parasite. This reduced replication is seen both for *Pb*A, which infects primarily reticulocytes, and *Pc*A, a parasite that infects both reticulocytes and RBCs (Figure 6; Deharo et al., 1996; Ott, 1968). This suggests that changes in the intracellular milieu caused by the loss of BPGM function and that are associated with reduced permissiveness to *Plasmodium* replication are expressed in both mature RBCs and reticulocytes (Lelliott et al., 2015; Stephens et al., 2012). Quantifying the two forms of the intracellular parasites (early ring-stage and late-stage parasites) suggests that the protective effect of the mutation is not through the reduced rate of infection of mutant RBCs, but rather affects

(B) Heatmap showing the normalized and corrected levels of the 50 metabolites most differentially altered in $Bpgm^{L166P}$ versus WT RBCs ($p \leq 0.05$). Each column represents the relative level value normalized (median normalized and log-transformed) and corrected for the metabolites interrogated for each WT (n = 5) and $Bpgm^{L166P}$ (n = 5) mice replicates.

(C) Volcano plot showing the relative fold change (FC) in the levels of the 134 metabolites quantified from WT and $Bpgm^{L166P}$ extracts. Each point represents the average value of the relative FC between the mutant and WT of 1 metabolite in 5 independent replicates. The relative FC cutoff was set at (FC) $\geq$ 1.5 ($\log_2$ FC of $\geq$0.53 [light gray broken vertical lines] and for an adjusted false discovery rate [FDR] of $\leq$0.05 [$-$log{adj p value} of $\geq$1.3], light gray broken horizontal line). Green and red dots indicate the overexpressed metabolites in WT and $Bpgm^{L166P}$ RBCs, respectively.

(D) Boxplot showing individual values of metabolites from purine and pyrimidine pathways identified in the metabolite enrichment set (Figures S7A and S7B) showing significant FC variations of steady-state levels between WT and mutants.

All of the data are shown as means ± SDs. Two-tailed unpaired Student's t test was used to calculate significance, and p values are indicated. The data are from a representative experiment from 2 independent experiments. Related to Figure S7 and Tables S1 and S2.

intraerythrocytic parasites, possibly due to an effect of the mutation on the RBC intracellular milieu. This reduced intraerythrocytic replication would translate into lower overall blood-stage parasitemia and resistance to both *Pb*A and *Pc*A infections. Our metabolite analysis identifies a major impact of the *Bpgm* mutation on several pathways (particularly purine metabolism), including severe reduction of tri-, di-, and monophosphate nucleotide (ATP/GTP) pools, which is indicative of reduced energy stores in the mutant. Reduced ATP/GTP levels caused by other erythroid mutations, including PKLR deficiency, have been associated with the reduced maturation and decreased intracellular replication of *Plasmodium* species in human and mouse RBCs (Ayi et al., 2009; Min-Oo et al., 2003). The *Plasmodium* genome is devoid of genes for the biosynthesis of purine nucleosides, and thus the parasite is unable to synthesize purines *de novo* (Downie et al., 2008), relying instead on the salvage of purines from the host RBCs via the conversion of adenosine and inosine to hypoxanthine (Downie et al., 2008). In addition, the parasite requires a considerable amount of triphosphate nucleotides to maintain its high metabolic rate. Hence, reduced parasite replication in *Bpgm* mutant RBCs may be explained in part by impaired purine metabolism and the reduced availability of ATP/GTP. Anti-plasmodial therapies based on targeting *Plasmodium* adenosine deaminase and purine nucleoside phosphorylase with nucleoside or nucleotide analogs have shown promising therapeutic value (Cassera et al., 2011; Dziekan et al., 2019). Finally, we cannot exclude the possibility that erythrocytes infected with mature forms of the PcA and PbA parasites are preferentially eliminated by the mutant reticuloendothelial system. Although our metabolomics data support a direct intrinsic RBC-specific effect of the mutation on parasite replication *in situ*, and although our cellular immunophenotyping data failed to detect differences between mutant and WT immune cell numbers and functions, additional experimentation aimed at characterizing the elimination of RBCs infected with different forms of the parasite by WT and mutant macrophages would be required to formally eliminate this possibility.

BPGM deficiency in humans is exceedingly rare, with only a few patients ever described (Cartier et al., 1972; Hoyer et al., 2004; Labie et al., 1970; Lemarchandel et al., 1992; Oliveira et al., 2018; Petousi et al., 2014; Rosa et al., 1978). Rosa et al. (1978) reported the first case of a patient with complete BPGM deficiency, presenting with erythrocytosis, elevated Hb (>190 g/L), and RBC 2,3-BPG levels <3% of controls. Genetically, the patient was compound heterozygote for a loss of function variant (R89C) and a single nucleotide deletion at codon 19 of the protein (Lemarchandel et al., 1992). Another patient with BPGM deficiency (homozygote for R62Q) with erythrocytosis was described, but in the context of additional G6PD deficiency (Hoyer et al., 2004). Finally, Oliveira et al. (2018) recently reported homozygosity for a novel BPGM variant at position 169 in a patient suffering from erythrocytosis. The clinical features of these very rare patients are similar to the phenotype of the $Bpgm^{L166P}$ mouse mutant reported here, establishing $Bpgm^{L166P}$ as a valid mouse model for the study of human BPGM deficiency.

Overall, a highlight of our study is how the loss of BPGM function protects against both CM and SMA, the two major causes of malaria-related morbidity and mortality in humans. Our finding establishes BPGM as a new example of erythroid-specific protein in which functional variants affect the susceptibility to malaria. Although our study only demonstrates this effect against murine parasites *Pb*A and *Pc*A, the list of such erythroid-specific genes and proteins include Hb (HbC, HbS, and HbE), G6PD, PKLR, SLC4A1, glycophorins, ABO blood groups, Duffy antigen (FY), and heme oxygenase (HO1) (Huang et al., 2018; Torre et al., 2018). The possibility that human BPGM deficiency may affect the replication of the human *Plasmodium* parasites (*P. falciparum*, *P. vivax*) in RBCs from rare BPGM-deficient patients remains to be tested and can reveal BPGM as a potential malaria therapeutic intervention point. Likewise, the possibility that genetic variants within or near the human *BPGM* gene affect susceptibility to malaria needs to be examined in field and population studies from areas of endemic disease.

STAR★METHODS

Detailed methods are provided in the online version of this paper and include the following:

- KEY RESOURCES TABLE
- RESOURCE AVAILABILITY
  - Lead Contact
  - Materials Availability
  - Data and Code Availability
- EXPERIMENTAL MODEL AND SUBJECT DETAILS
  - Mice and Ethics Statement
  - Cell Lines and Cell Culture
- METHOD DETAILS
  - Whole-Exome Sequencing
  - Parasites and Infection
  - BPGM Protein Expression and Stability
  - BPGM Sequence Alignments
  - LC-MS Quantification of 2,3-BPG
  - P50 Measurement
  - Erythroid Cells Analyses
  - Evans Blue Dye Extravasation
  - Cellular Immunophenotyping
  - EPO Quantification
  - Treatment with Phenylhydrazine
  - Metabolite Profiling
- QUANTIFICATION AND STATISTICAL ANALYSIS

SUPPLEMENTAL INFORMATION

Supplemental Information can be found online at https://doi.org/10.1016/j.celrep.2020.108170.

ACKNOWLEDGMENTS

This work was supported by a foundation research grant to P.G. from the Canadian Institutes of Health Research and from the Canadian Institute for Advanced Research (Human and the Microbiome Program). P.G. receives salary support from a Distinguished James McGill Professorship Award. S.L. is an FRQ-S Research Scholars Emeritus awardee. A.F. holds a scholarship from the Département de Microbiologie, Infectiologie et Immunologie at the University of Montréal. Metabolite profiling was carried out at the Goodman Cancer Research Center's Metabolomics Innovation Resource, which is funded in part by the Dr. John R. and Clara M. Fraser Memorial Trust, the Terry

Fox Foundation, the Québec Breast Cancer Foundation, and McGill University. The authors are indebted to Susan Gauthier and Geneviève Perreault (McGill University) for expert technical assistance; to Tatiana Scorza (Université) for valuable discussions; and to Kevin Kain (University of Toronto), Georges E. Rivard (Ste-Justine Hospital), and Maria J. Polyak (McGill University) for expert advice and assistance.

AUTHOR CONTRIBUTIONS

R.V.B. and C.O.G. contributed to the identification of the ENU-induced mutations. N.M. performed the Evans blue dye extravasation assay. A.F., S.L., D.V., H.G., J.T.P., and N.F. contributed to the blood gas analysis. J.T.P. contributed to the concept, guided the p50 analysis, and edited the manuscript. N.F., M.T.R., and D.Z.A. contributed to the metabolomic analysis. N.F. and G.D. analyzed the metabolomic dataset. All of the protein modeling was done by A. Bassenden and A. Berghuis. N.F., W.L., J.R., and T.M. contributed to the liquid chromatography-mass spectrometry (LC-MS) data. N.F., M.T., and M.S. provided guidance on the mouse models of blood-stage malaria and the study of RBC precursors. S.M.V. and P.G. designed and supervised the ENU-mutagenesis screens. G.X. performed all of the other steady-state, *Pb*A, *Pc*A, and PHZ experiments. The analysis and figures were done by G.X. and N.F. G.X., N.F., and P.G. wrote the manuscript. All of the authors provided helpful comments.

DECLARATION OF INTERESTS

The authors declare no competing interests.

Received: September 11, 2019
Revised: July 7, 2020
Accepted: August 27, 2020
Published: September 22, 2020

REFERENCES

Abdalla, S., Weatherall, D.J., Wickramasinghe, S.N., and Hughes, M. (1980). The anaemia of P. falciparum malaria. Br. J. Haematol. *46*, 171–183.

Agarwal, N., Mojica-Henshaw, M.P., Simmons, E.D., Hussey, D., Ou, C.N., and Prchal, J.T. (2007). Familial polycythemia caused by a novel mutation in the beta globin gene: essential role of P50 in evaluation of familial polycythemia. Int. J. Med. Sci. *4*, 232–236.

Ayi, K., Min-Oo, G., Serghides, L., Crockett, M., Kirby-Allen, M., Quirt, I., Gros, P., and Kain, K.C. (2008). Pyruvate kinase deficiency and malaria. N. Engl. J. Med. *358*, 1805–1810.

Ayi, K., Liles, W.C., Gros, P., and Kain, K.C. (2009). Adenosine triphosphate depletion of erythrocytes simulates the phenotype associated with pyruvate kinase deficiency and confers protection against Plasmodium falciparum in vitro. J. Infect. Dis. *200*, 1289–1299.

Band, G., Rockett, K.A., Spencer, C.C., and Kwiatkowski, D.P.; Malaria Genomic Epidemiology Network (2015). A novel locus of resistance to severe malaria in a region of ancient balancing selection. Nature *526*, 253–257.

Berghout, J., Higgins, S., Loucoubar, C., Sakuntabhai, A., Kain, K.C., and Gros, P. (2012). Genetic diversity in human erythrocyte pyruvate kinase. Genes Immun. *13*, 98–102.

Bongfen, S.E., Rodrigue-Gervais, I.-G., Berghout, J., Torre, S., Cingolani, P., Wiltshire, S.A., Leiva-Torres, G.A., Letourneau, L., Sladek, R., Blanchette, M., et al. (2012). An N-ethyl-N-nitrosourea (ENU)-induced dominant negative mutation in the JAK3 kinase protects against cerebral malaria. PLOS ONE *7*, e31012.

Caignard, G., Eva, M.M., van Bruggen, R., Eveleigh, R., Bourque, G., Malo, D., Gros, P., and Vidal, S.M. (2014). Mouse ENU Mutagenesis to Understand Immunity to Infection: Methods, Selected Examples, and Perspectives. Genes (Basel) *5*, 887–925.

Cartier, P., Labie, D., Leroux, J.P., Najman, A., and Demaugre, F. (1972). [Familial diphosphoglycerate mutase deficiency: hematological and biochemical study]. Nouv. Rev. Fr. Hematol. *12*, 269–287.

Cassera, M.B., Zhang, Y., Hazleton, K.Z., and Schramm, V.L. (2011). Purine and pyrimidine pathways as targets in Plasmodium falciparum. Curr. Top. Med. Chem. *11*, 2103–2115.

Chang, K.-H., and Stevenson, M.M. (2004). Malarial anaemia: mechanisms and implications of insufficient erythropoiesis during blood-stage malaria. Int. J. Parasitol. *34*, 1501–1516.

Chen, K., Liu, J., Heck, S., Chasis, J.A., An, X., and Mohandas, N. (2009). Resolving the distinct stages in erythroid differentiation based on dynamic changes in membrane protein expression during erythropoiesis. Proc. Natl. Acad. Sci. USA *106*, 17413–17418.

Chu, W.-T., Zheng, Q.-C., and Zhang, H.-X. (2014). Insights into the phosphatase and the synthase activities of human bisphosphoglycerate mutase: a quantum mechanics/molecular mechanics simulation. Phys. Chem. Chem. Phys. *16*, 3946–3954.

Cowman, A.F., Healer, J., Marapana, D., and Marsh, K. (2016). Malaria: Biology and Disease. Cell *167*, 610–624.

Craescu, C.T., Schaad, O., Garel, M.C., Rosa, R., and Edelstein, S. (1992). Structural modeling of the human erythrocyte bisphosphoglycerate mutase. Biochimie *74*, 519–526.

Culleton, R.L., Mita, T., Ndounga, M., Unger, H., Cravo, P.V., Paganotti, G.M., Takahashi, N., Kaneko, A., Eto, H., Tinto, H., et al. (2008). Failure to detect Plasmodium vivax in West and Central Africa by PCR species typing. Malar. J. *7*, 174.

de Koning-Ward, T.F., Dixon, M.W.A., Tilley, L., and Gilson, P.R. (2016). Plasmodium species: master renovators of their host cells. Nat. Rev. Microbiol. *14*, 494–507.

Deharo, E., Coquelin, F., Chabaud, A.G., and Landau, I. (1996). The erythrocytic schizogony of two synchronized strains of plasmodium berghei, NK65 and ANKA, in normocytes and reticulocytes. Parasitol. Res. *82*, 178–182.

Downie, M.J., Kirk, K., and Mamoun, C.B. (2008). Purine salvage pathways in the intraerythrocytic malaria parasite Plasmodium falciparum. Eukaryot. Cell *7*, 1231–1237.

Dziekan, J.M., Yu, H., Chen, D., Dai, L., Wirjanata, G., Larsson, A., Prabhu, N., Sobota, R.M., Bozdech, Z., and Nordlund, P. (2019). Identifying purine nucleoside phosphorylase as the target of quinine using cellular thermal shift assay. Sci. Transl. Med. *11*, eaau3174.

Fowkes, F.J.I., Allen, S.J., Allen, A., Alpers, M.P., Weatherall, D.J., and Day, K.P. (2008). Increased microerythrocyte count in homozygous α(+)-thalassaemia contributes to protection against severe malarial anaemia. PLOS Med. *5*, e56.

Genton, B., al-Yaman, F., Mgone, C.S., Alexander, N., Paniu, M.M., Alpers, M.P., and Mokela, D. (1995). Ovalocytosis and cerebral malaria. Nature *378*, 564–565.

Ghazanfari, N., Mueller, S.N., and Heath, W.R. (2018). Cerebral Malaria in Mouse and Man. Front. Immunol. *9*, 2016.

Goheen, M.M., Campino, S., and Cerami, C. (2017). The role of the red blood cell in host defence against falciparum malaria: an expanding repertoire of evolutionary alterations. Br. J. Haematol. *179*, 543–556.

Hernandez-Valladares, M., Naessens, J., and Iraqi, F.A. (2005). Genetic resistance to malaria in mouse models. Trends Parasitol. *21*, 352–355.

Hong, W.-J., and Gotlib, J. (2014). Hereditary erythrocytosis, thrombocytosis and neutrophilia. Best Pract. Res. Clin. Haematol. *27*, 95–106.

Howland, S.W., Claser, C., Poh, C.M., Gun, S.Y., and Rénia, L. (2015). Pathogenic CD8+ T cells in experimental cerebral malaria. Semin. Immunopathol. *37*, 221–231.

Hoyer, J.D., Allen, S.L., Beutler, E., Kubik, K., West, C., and Fairbanks, V.F. (2004). Erythrocytosis due to bisphosphoglycerate mutase deficiency with concurrent glucose-6-phosphate dehydrogenase (G-6-PD) deficiency. Am. J. Hematol. *75*, 205–208.

Huang, H.M., McMorran, B.J., Foote, S.J., and Burgio, G. (2018). Host genetics in malaria: lessons from mouse studies. Mamm. Genome *29*, 507–522.

Jarolim, P., Palek, J., Amato, D., Hassan, K., Sapak, P., Nurse, G.T., Rubin, H.L., Zhai, S., Sahr, K.E., and Liu, S.C. (1991). Deletion in erythrocyte band 3 gene in malaria-resistant Southeast Asian ovalocytosis. Proc. Natl. Acad. Sci. USA *88*, 11022–11026.

Kennedy, J.M., Fodil, N., Torre, S., Bongfen, S.E., Olivier, J.-F., Leung, V., Langlais, D., Meunier, C., Berghout, J., Langat, P., et al. (2014). CCDC88B is a novel regulator of maturation and effector functions of T cells during pathological inflammation. J. Exp. Med. *211*, 2519–2535.

Koulnis, M., Pop, R., Porpiglia, E., Shearstone, J.R., Hidalgo, D., and Socolovsky, M. (2011). Identification and analysis of mouse erythroid progenitors using the CD71/TER119 flow-cytometric assay. J. Vis. Exp. (*54*), 2809.

Kundu, A., Bag, S., Ramaiah, S., and Anbarasu, A. (2013). Leucine to proline substitution by SNP at position 197 in Caspase-9 gene expression leads to neuroblastoma: a bioinformatics analysis. 3 Biotech *3*, 225–234.

Labie, D., Leroux, J., Najman, A., and Reyrolle, C. (1970). Familial diphosphoglyceratemutase deficiency. Influence on the oxygen affinity curves of hemoglobin. FEBS Lett. *9*, 37–40.

Lamikanra, A.A., Brown, D., Potocnik, A., Casals-Pascual, C., Langhorne, J., and Roberts, D.J. (2007). Malarial anemia: of mice and men. Blood *110*, 18–28.

Langlais, D., Fodil, N., and Gros, P. (2017). Genetics of Infectious and Inflammatory Diseases: Overlapping Discoveries from Association and Exome-Sequencing Studies. Annu. Rev. Immunol. *35*, 1–30.

Lelliott, P.M., McMorran, B.J., Foote, S.J., and Burgio, G. (2015). The influence of host genetics on erythrocytes and malaria infection: is there therapeutic potential? Malar. J. *14*, 289.

Lemarchandel, V., Joulin, V., Valentin, C., Rosa, R., Galactéros, F., Rosa, J., and Cohen-Solal, M. (1992). Compound heterozygosity in a complete erythrocyte bisphosphoglycerate mutase deficiency. Blood *80*, 2643–2649.

Li, H., and Durbin, R. (2009). Fast and accurate short read alignment with Burrows-Wheeler transform. Bioinformatics *25*, 1754–1760.

Lichtman, M.A., Murphy, M.S., and Adamson, J.W. (1976). Detection of mutant hemoglobins with altered affinity for oxygen. A simplified technique. Ann. Intern. Med. *84*, 517–520.

Liu, Y., Pop, R., Sadegh, C., Brugnara, C., Haase, V.H., and Socolovsky, M. (2006). Suppression of Fas-FasL coexpression by erythropoietin mediates erythroblast expansion during the erythropoietic stress response in vivo. Blood *108*, 123–133.

Louicharoen, C., Patin, E., Paul, R., Nuchprayoon, I., Witoonpanich, B., Peerapittayamongkol, C., Casademont, I., Sura, T., Laird, N.M., Singhasivanon, P., et al. (2009). Positively selected G6PD-Mahidol mutation reduces Plasmodium vivax density in Southeast Asians. Science *326*, 1546–1549.

Malleret, B., Claser, C., Ong, A.S.M., Suwanarusk, R., Sriprawat, K., Howland, S.W., Russell, B., Nosten, F., and Rénia, L. (2011). A rapid and robust tri-color flow cytometry assay for monitoring malaria parasite development. Sci. Rep. *1*, 118.

Malleret, B., Li, A., Zhang, R., Tan, K.S.W., Suwanarusk, R., Claser, C., Cho, J.S., Koh, E.G.L., Chu, C.S., Pukrittayakamee, S., et al. (2015). Plasmodium vivax: restricted tropism and rapid remodeling of CD71-positive reticulocytes. Blood *125*, 1314–1324.

Miller, L.H., Mason, S.J., Clyde, D.F., and McGinniss, M.H. (1976). The resistance factor to Plasmodium vivax in blacks. The Duffy-blood-group genotype, FyFy. N. Engl. J. Med. *295*, 302–304.

Min-Oo, G., Fortin, A., Tam, M.F., Nantel, A., Stevenson, M.M., and Gros, P. (2003). Pyruvate kinase deficiency in mice protects against malaria. Nat. Genet. *35*, 357–362.

Mishra, S.K., and Newton, C.R.J.C. (2009). Diagnosis and management of the neurological complications of falciparum malaria. Nat. Rev. Neurol. *5*, 189–198.

Moradin, N., Torre, S., Gauthier, S., Tam, M., Hawari, J., Vandercruyssen, K., De Spiegeleer, B., Fortin, A., Stevenson, M.M., and Gros, P. (2016). Cysteamine broadly improves the anti-plasmodial activity of artemisinins against murine blood stage and cerebral malaria. Malar. J. *15*, 260.

Oliveira, J.L., Coon, L.M., Frederick, L.A., Hein, M., Swanson, K.C., Savedra, M.E., Porter, T.R., Patnaik, M.M., Tefferi, A., Pardanani, A., et al. (2018). Genotype-Phenotype Correlation of Hereditary Erythrocytosis Mutations, a single center experience. Am. J. Hematol. *93*, 1029–1041.

Oslund, R.C., Su, X., Haugbro, M., Kee, J.-M., Esposito, M., David, Y., Wang, B., Ge, E., Perlman, D.H., Kang, Y., et al. (2017). Bisphosphoglycerate mutase controls serine pathway flux via 3-phosphoglycerate. Nat. Chem. Biol. *13*, 1081–1087.

Ott, K.J. (1968). Influence of reticulocytosis on the course of infection of *Plasmodium chabaudi* and *P. berghei*. J. Protozool. *15*, 365–369.

Patterson, A., Price, N.C., and Nairn, J. (2010). Unliganded structure of human bisphosphoglycerate mutase reveals side-chain movements induced by ligand binding. Acta Crystallogr. Sect. F Struct. Biol. Cryst. Commun. *66*, 1415–1420.

Petousi, N., Copley, R.R., Lappin, T.R., Haggan, S.E., Bento, C.M., Cario, H., Percy, M.J., Ratcliffe, P.J., Robbins, P.A., and McMullin, M.F.; WGS Consortium (2014). Erythrocytosis associated with a novel missense mutation in the BPGM gene. Haematologica *99*, e201–e204.

Prchal, J.T., and Gregg, X.T. (2005). Red cell enzymes. Hematology Am. Soc. Hematol. Educ. Program (*1*), 19–23.

Pritlove, D.C., Gu, M., Boyd, C.A.R., Randeva, H.S., and Vatish, M. (2006). Novel placental expression of 2,3-bisphosphoglycerate mutase. Placenta *27*, 924–927.

Quinlan, A.R., and Hall, I.M. (2010). BEDTools: a flexible suite of utilities for comparing genomic features. Bioinformatics *26*, 841–842.

Rasti, N., Wahlgren, M., and Chen, Q. (2004). Molecular aspects of malaria pathogenesis. FEMS Immunol. Med. Microbiol. *41*, 9–26.

Rosa, R., Prehu, M.O., Beuzard, Y., and Rosa, J. (1978). The first case of a complete deficiency of diphosphoglycerate mutase in human erythrocytes. J. Clin. Invest. *62*, 907–915.

Stephens, R., Culleton, R.L., and Lamb, T.J. (2012). The contribution of Plasmodium chabaudi to our understanding of malaria. Trends Parasitol. *28*, 73–82.

Stevenson, M.M., Lyanga, J.J., and Skamene, E. (1982). Murine malaria: genetic control of resistance to Plasmodium chabaudi. Infect. Immun. *38*, 80–88.

Taylor, S.M., Parobek, C.M., and Fairhurst, R.M. (2012). Haemoglobinopathies and the clinical epidemiology of malaria: a systematic review and meta-analysis. Lancet Infect. Dis. *12*, 457–468.

Torre, S., Faucher, S.P., Fodil, N., Bongfen, S.E., Berghout, J., Schwartzentruber, J.A., Majewski, J., Lathrop, M., Cooper, A.M., Vidal, S.M., and Gros, P. (2015). THEMIS is required for pathogenesis of cerebral malaria and protection against pulmonary tuberculosis. Infect. Immun. *83*, 759–768.

Torre, S., Polyak, M.J., Langlais, D., Fodil, N., Kennedy, J.M., Radovanovic, I., Berghout, J., Leiva-Torres, G.A., Krawczyk, C.M., Ilangumaran, S., et al. (2017). USP15 regulates type I interferon response and is required for pathogenesis of neuroinflammation. Nat. Immunol. *18*, 54–63.

Torre, S., Langlais, D., and Gros, P. (2018). Genetic analysis of cerebral malaria in the mouse model infected with Plasmodium berghei. Mamm. Genome *29*, 488–506.

van Bruggen, R., Gualtieri, C., Iliescu, A., Louicharoen Cheepsunthorn, C., Mungkalasut, P., Trape, J.-F., Modiano, D., Sirima, B.S., Singhasivanon, P., Lathrop, M., et al. (2015). Modulation of Malaria Phenotypes by Pyruvate Kinase (PKLR) Variants in a Thai Population. PLOS ONE *10*, e0144555.

van Wijk, R., and van Solinge, W.W. (2005). The energy-less red blood cell is lost: erythrocyte enzyme abnormalities of glycolysis. Blood *106*, 4034–4042.

Wang, Y., Wei, Z., Bian, Q., Cheng, Z., Wan, M., Liu, L., and Gong, W. (2004). Crystal structure of human bisphosphoglycerate mutase. J. Biol. Chem. *279*, 39132–39138.

Wang, K., Li, M., and Hakonarson, H. (2010). ANNOVAR: functional annotation of genetic variants from high-throughput sequencing data. Nucleic Acids Res. *38*, e164.

Weiss, L., Johnson, J., and Weidanz, W. (1989). Mechanisms of splenic control of murine malaria: tissue culture studies of the erythropoietic interplay of spleen, bone marrow, and blood in lethal (strain 17XL) Plasmodium yoelii malaria in BALB/c mice. Am. J. Trop. Med. Hyg. *41*, 135–143.

White, N.J. (2018). Anaemia and malaria. Malar. J. *17*, 371.

White, N.J., Pukrittayakamee, S., Hien, T.T., Faiz, M.A., Mokuolu, O.A., and Dondorp, A.M. (2014). Malaria. Lancet *383*, 723–735.

Wickramasinghe, S.N., Looareesuwan, S., Nagachinta, B., and White, N.J. (1989). Dyserythropoiesis and ineffective erythropoiesis in Plasmodium vivax malaria. Br. J. Haematol. *72*, 91–99.

World Health Organization (2018). World Malaria Report 2018. https://www.who.int/malaria/publications/world-malaria-report-2018/en/.

Xia, J., Sinelnikov, I.V., Han, B., and Wishart, D.S. (2015). MetaboAnalyst 3.0–making metabolomics more meaningful. Nucleic Acids Res. *43*, W251–W257.

Yap, G.S., and Stevenson, M.M. (1992). Plasmodium chabaudi AS: erythropoietic responses during infection in resistant and susceptible mice. Exp. Parasitol. *75*, 340–352.

STAR★METHODS

KEY RESOURCES TABLE

REAGENT or RESOURCE	SOURCE	IDENTIFIER
Antibodies		
Rabbit polyclonal anti-BPGM	Abcam	Cat. #: ab97497; RRID: AB_10680066
Mouse monoclonal anti-FLAG	Sigma-Aldrich	Cat. #: F1804; RRID: AB_262044
Anti-mouse CD16/32 (clone: 93)	BioLegend	Cat. #: 101302; RRID: AB_312801
Anti-mouse Ter-119 (clone: Ter-119), APC	eBioscience	Cat. #: 17-5921-82; RRID: AB_469473
Anti-mouse CD45 (clone: 30-F11), APC-eFluor 780	eBioscience	Cat. #: 47-0451-82; RRID: AB_1548781
Anti-mouse CD71 (Transferrin Receptor) (clone: R17217), PE	eBioscience	Cat. #: 12-0711-81; RRID: AB_465739
Anti-mouse/human CD11b (clone: M1/70), BV421	BioLegend	Cat. #: 101235; RRID: AB_10897942
Anti-mouse/human B220 (clone: RA3-6B2), BV421	BioLegend	Cat. #: 103251; RRID: AB_2562905
Anti-mouse Ly-6G (clone: 1A8), PerCP/Cy5.5	BioLegend	Cat. #: 127615; RRID: AB_1877272
Anti-mouse Ly-6G (clone 1A8), FITC	BioLegend	Cat. #:127605; RRID: AB_1236488
Anti-mouse F4/80 (clone: BM8), PE-Cy5	eBioscience	Cat. #: 15-4801-80; RRID: AB_468797
Anti-mouse CD11c (clone: N418), PE	eBioscience	Cat. #: 12-0114-81; RRID: AB_465551
Anti-mouse Ly-6C (clone: HK1.4), FITC	BioLegend	Cat. #: 128005; RRID: AB_1186134
Anti-mouse Ly-6C (clone: HK1.4) PE	eBioscience	Cat. #: 12-5932-82; RRID: AB_10804510
Anti-mouse TCRß (clone: H57-597), PE	eBioscience	Cat. #: 12-5961-81; RRID: AB_466065
Anti-mouse TCRß (clone H57-597), FITC	eBioscience	Cat. #: 11-5961-82; RRID: AB_465323
Anti-mouse CD335 (NKp46) (clone: 29A1.4), APC	eBioscience	Cat. #: 17-3351-80; RRID: AB_2815089
Anti-mouse CD4 (clone: RM4-5), PerCP-Cy5.5	eBioscience	Cat. #: 45-0042-80; RRID: AB_906231
Anti-mouse CD8a (clone: 53-6.7), Alexa Fluor 700	eBioscience	Cat. #: 56-0081-80; RRID: AB_494006
Anti-mouse CD8a (clone: 53-6.7), PE	eBioscience	Cat. #: 12-0081-82; RRID: AB_465530
Anti-mouse CD11b (M1/70), APC	eBioscience	Cat. #: 17-0112-82; RRID: AB_469343
Anti-mouse CD19 (clone: 6D5), BV421	BioLegend	Cat. #: 115549; RRID: AB_2563066
Bacterial and Virus Strains		
DH5-alpha Competent *E. coli*	ThermoFisher Scientific	Cat.#: 18265017
Chemicals, Peptides, and Recombinant Proteins		
Phenylhydrazine hydrochloride	Sigma-Aldrich	Cat. #: 114715
Zombie Aqua Fixable Viability Kit	BioLegend	Cat. #: 423102
N-ethyl *N*-nitrosourea	Sigma-Aldrich	Cat. #: N3385
Evans Blue Dye	Sigma-Aldrich	Cat. #: E2129
Hoechst 33342	Invitrogen	Cat. #: H3570
Cycloheximide	Sigma-Aldrich	Cat. #: C7698
Lipofectamine 2000 reagent	ThermoFisher	Cat. #: 11668019
MboII Restriction Endonuclease	New England BioLabs	Cat. #: R0148
Geneticin (G418)	ThermoFisher	Cat. #: 11811031
Critical Commercial Assays		
SureSelectXT Mouse All Exon	Agilent Technologies	Cat. #: 5190
Mouse Erythropoietin Quantikine ELISA kit	R&D Systems	Cat. #: MEP00B

(*Continued on next page*)

Continued

REAGENT or RESOURCE	SOURCE	IDENTIFIER
Experimental Models: Cell Lines		
Human: HEK293	ATCC	Cat. #: CRL-1573; RRID: CVCL_0045
Flag-WT BPGM^{L166} HEK293	This paper	N/A
Flag-BPGM^{P166} HEK293	This paper	N/A
Experimental Models: Organisms/Strains		
Mouse: C57BL/6	The Jackson Laboratory	000664
Mouse: *Bpgm*^{L166P} (C57BL/6 background)	Bred in house	N/A
Mouse: A/J	The Jackson Laboratory	000646
Mouse: *Bpgm*^{L166P} (A/J background)	Bred in house	N/A
Parasite: *Plasmodium berghei* ANKA	Originally obtained from MR4	N/A
Parasite: *Plasmodium chabaudi chabaudi* AS	Originally obtained from MR4	N/A
Oligonucleotides		
Primer for *Bpgm*^{L166P} F (Genotyping): CTGAATGAGCGTCACTATGG	This paper	N/A
Primer for *Bpgm*^{L166P} R (Genotyping): GTACCTCCCCAATTCTGAAAC	N/A	N/A
Primer for *Bpgm*^{L166P} F (Site-directed mutagenesis): GGATGTTCTGG AGAGACTTCCTCCCTACTGGAAGG	This paper	N/A
Primer for *Bpgm*^{L166P} R (Site-directed mutagenesis): CCTTCCAGTAGGGA GGAAGTCTCTCCAGAACATCC	This paper	N/A
Recombinant DNA		
pCMV6-Myc-DDK- WT BPGM^{L166}	Origene	Cat. #: MR203358
pCMV6-Myc-DDK- BPGM^{P166}	This paper	N/A
Software and Algorithms		
FlowJo Version 10	Tree Star	N/A
GraphPad Prism Version 6	GraphPad	N/A
Jalview Alias	Jalview	http://www.jalview.org/
FIJI- ImageJ	ImageJ	https://imagej.net/Fiji
BEDTools	Quinlan and Hall, 2010	https://bedtools.readthedocs.io/en/latest/
Annovar	Wang et al., 2010	https://doc-openbio.readthedocs.io/projects/annovar/en/latest/
PyMOL	Patterson et al., 2010	https://pymol.org/2/
Samtools	Li and Durbin, 2009	http://samtools.sourceforge.net/
MetaboAnalyst 3.0	Xia et al., 2015	https://www.metaboanalyst.ca/
Burrows-Wheeler alignment tool	Li and Durbin, 2009	http://bio-bwa.sourceforge.net/

RESOURCE AVAILABILITY

Lead Contact

Further information and requests for resources and reagents should be directed to and will be fulfilled by the Lead Contact, Philippe Gros (philippe.gros@mcgill.ca).

Materials Availability

All reagents generated in this study are available upon request to the Lead Contact but may require a completed Materials Transfer Agreement if there is potential for commercial application.

Data and Code Availability

The published article includes all metabolomic datasets generated and analyzed for this study in Tables S1 and S2.

EXPERIMENTAL MODEL AND SUBJECT DETAILS

Mice and Ethics Statement

ENU-mutagenesis and breeding of informative pedigrees were performed as previously described (Kennedy et al., 2014; Torre et al., 2017). Inbred mice were purchased from Jackson laboratories (Bar Harbor, ME). In addition to the originating C57BL/6 (B6) background (backcrossed to B6 for 4 additional generations), the *Bpgm*^{L166P} mutation was backcrossed onto the A/J genetic background (four consecutive backcrosses) to generate the A/J.*Bpgm*^{L166P} mouse line. WT B6 or A/J mice were used as controls. All experiments were performed with 8–13 weeks old mice that were age- and sex- matched. Genotyping of *Bpgm*^{L166P} mice were performed using standard PCR amplification on genomic DNA with primers 5′-CTGAATGAGCGTCACTATGG-3′ and 5′-GTACCTCCCCAATTCT GAAAC-3′ primers, followed by restriction enzyme digestion with MboII (New England BioLabs), and gel electrophoresis (*Bpgm*^{L166P} homozygotes displaying a single band of 607bp). Experiments were performed in accordance with the regulations of the Canadian Council on Animal Care. All protocols were approved by the Animal Care Committee of McGill University (protocol: 5287).

Cell Lines and Cell Culture

HEK293 cells (ATCC CRL-1573) were used for the generation of stably transfected cell lines expressing either the WT BPGM^{L166} or mutant BPGM^{P166} variants. Cells were maintained in Dulbecco's Modified Eagle Medium (DMEM; Wisent) supplemented with 10% heat inactivated Fetal Bovine Serum (FBS) (GIBCO) and 100U/mL of Penicillin/Streptomycin (Hyclone) at 37°C with 5% CO_2. For culture of stably transfected cells, plasmid containing full-length mouse *Bpgm* cDNA obtained from Origene was used (Cat#: MR203358) as template for generation of BPGM^{P166} protein variant through site-directed mutagenesis. 5′- GGATGTTCTGGAGAG ACTTCCTCCCTACTGGAAGG −3′ and 5′- CCTTCCAGTAGGGAGGAAGTC TCTCC AGAACATCC −3′ primers were used. All cDNA constructs were verified by Sanger sequencing. For protein stability studies, HEK293 cells (ATCC CRL-1573) were transfected with flag-tagged WT BPGM^{L166} and BPGM^{P166} murine constructs using Lipofectamine 2000 reagent (ThermoFisher). Stably transfected cells were generated following clonal selection and expansion in Geneticin (G418, 500ug/mL; ThermoFisher). All clones were verified by immunoblot using rabbit polyclonal anti-BPGM antibody (Abcam, ab97497; 1:500) and mouse monoclonal anti-flag antibody (1:2000; Sigma-Aldrich, F1804-1MG).

METHOD DETAILS

Whole-Exome Sequencing

Exome capture was performed using SureSelect Mouse All Exon kit (Agilent Technologies) and parallel sequencing on Illumina HiSeq 2000 (100-bp paired-end reads). Reads were aligned with mouse genome assembly July 2007 (NCBI37/mm9) by Burrows-Wheeler alignment tool (Li and Durbin, 2009). Coverage was assessed using BEDTools (Quinlan and Hall, 2010). Variants were called using Samtools pileup and varFilter, and annotated using Annovar (Li and Durbin, 2009; Wang et al., 2010).

Parasites and Infection

Parasite strains used in this study are *P. berghei* ANKA (*Pb*A) or *P. chabaudi chabaudi* AS (*Pc*A). All *Pb*A and *Pc*A parasites were maintained as frozen stocks at −80°C and routinely passaged in B6 or A/J mice to prepare infectious doses, as described (Bongfen et al., 2012). Blood parasitemia was determined on thin blood smears stained with Diff-Quik reagents (Sigma Aldrich). Male and female mice were infected with 10^6 *Pb*A pRBCs intravenously (i.v.; 0.2 mL), and were monitored three times daily for the appearance of neurological symptoms of CM, which occurred typically within 5-8 days (Torre et al., 2015, 2017). Mutant mice remaining symptom-free and surviving to d13 p.i. were considered to be ECM-resistant (Torre et al., 2015, 2017). For infection with *Pc*A, female mice were infected with 10^4 *Pc*A pRBC i.v. and blood parasitemia was monitored daily on thin blood smears.

BPGM Protein Expression and Stability

Tissue and cell lysates were prepared in 20mM Tris-HCL pH 8, 150mM of KCL, 10% glycerol, 5mM $MgCl_2$ and 0.1% Np-40, and dissolved in 1X Laemmli sample buffer and separated by electrophoresis on a 10% SDS-PAGE gel. BPGM protein expression was monitored by immunoblotting using a rabbit polyclonal anti-BPGM antibody (1:500; Abcam, ab97497). To examine protein stability, stably-transfected HEK293 cells expressing either wild-type BPGM^{L166} or the mutant BPGM^{P166} variant were treated with cycloheximide (100ug/mL; Sigma-Aldrich) for 2, 4, 6, 8, 12h, at which point cell lysates were prepared and analyzed by immunoblotting (anti-Flag antibody, 1:7000; Sigma-Aldrich, F1804-1MG). The L166 and P166 protein variants were modeled using the unliganded structure of human BPGM (PDB: 3NFY) using PyMOL (Patterson et al., 2010).

BPGM Sequence Alignments

L166 amino acid conservation in BPGM was generated using Jalview multiple sequence alignment. Sequences were obtained from UniProt (UniProtKB: P07738, P07952, P15327, Q3T014, Q4R6L7).

LC-MS Quantification of 2,3-BPG

Transfected BPGM^{L166} and BPGM^{P166} cells were grown in DMEM media supplemented with 10% FBS on a 10cm dish until confluency. Blood was collected in heparin coated tubes (Sarstedt) from WT and *Bpgm*^{L166P} mice, and the mouse plasma was removed from the heparinized whole blood by centrifugation. Both HEK293 cells and RBCs were resuspended in dry-iced 80% methanol (MeOH) containing 0.5% formic acid and neutralized with 15% ammonium bicarbonate (NH_4HCO_3). The supernatants were collected after a centrifugation at 17,000 × *g* for 5 min. The RBC lysates were subjected to an extra protein depletion Spin Columns (10Ksin column, BioVision). Samples were dried using a refrigerated SpeedVac overnight and stored at −80°C until analysis. The LC-MS method for the quantification of 2,3-BPG used reversed-phase ion-pairing chromatography coupled with negative mode electrospray ionization to a stand-alone orbitrap mass spectrometer (Thermo Scientific) scanning from m/z 85-1,000 at 1Hz at 100,000 resolution with LC separation on a Atlantis T3 column (150 mm × 2.1 mm, 3 μm particle size, 100 Å pore size, Waters) using a gradient of solvent A (97%:3% H_2O:MeOH with 10 mM tributylamine and 15 mM acetic acid), and solvent B (100% MeOH). The LC gradient was, 0 min, 0% B, 200 μl/min; 2 min, 0% B, 200 μl/min; 4 min, 20% B, 200 μl/min; 13 min, 80% B, 200 μl/min; 17 min, 100% B, 200 μl/min; 17.5 min, 100% B, 300 μl/min; 20 min, 100% B, 300 μl/min; 20.5 min, 0% B, 300 μl/min; 24 min, 0% B, 300 μl/min; 25 min, 0% B, 200 μl/min. Other LC parameters were column temperature at 25°C, autosampler temperature at 5°C, and injection volume of 15 μL.

P50 Measurement

Venous blood was collected in heparinized capillary tubes from the submandibular vein and placed on ice and processed within 10 min after collection. The whole blood samples were injected into the GEM Premier 5000 analyzer (Instrumentation Laboratory, MA 01730, United States) for the determination of blood gases. The pH, oxygen partial pressure (pO2) and oxygen saturation (SO2) values were then determined electrochemically and venous oxygen tension and oxygen saturation were used to determine the P50 (Agarwal et al., 2007; Lichtman et al., 1976).

Erythroid Cells Analyses

Whole blood was collected in EDTA tubes (Sarstedt), and hematological parameters were determined by standard automated methods. Erythroid differentiation was analyzed by FACS prior to and 6 days p.i. with *Pb*A and 10 days p.i. with *Pc*A. Single cell suspensions from spleen and bone marrow were prepared in Phosphate buffer saline (PBS) (Hyclone) containing 10% FBS (GIBCO) and 2mM EDTA (Invitrogen). 2.5 × 10^6 cells were blocked with anti-CD16/anti-CD32 (1:300, BioLegend) and stained with APC anti-Ter-119 (clone Ter-119, 1:200, eBioscience), APC-eflouro 780 anti-CD45 (clone 30-F11, 1:400, eBioscience), PE anti-CD71 (clone R17217, 1:200, eBioscience) for 30mins at 4°C. Non-viable cells were excluded using Zombie Aqua Dye-V500 (7-AAD) (1:400, BioLegend). Data was acquired with a BD LSR Fortessa and analyzed using FlowJo software (Tree Star). Monitoring intra-erythrocytic parasite development by FACS was performed as described (Malleret et al., 2011, 2015). Briefly, on d6 p.i. with *Pb*A or on d7 p.i. with *Pc*A, near peak parasitemia, fresh whole blood was collected by cardiac puncture in EDTA containing tubes. 2.5uL of blood was stained (20°C, 25mins) with Hoechst 33342 (Invitrogen) at a final concentration of 5ug/mL, followed by staining for erythroid cells (Ter-119, CD71) as described (see above), followed by flow cytometry.

Evans Blue Dye Extravasation

The integrity of the blood brain barrier in *Pb*A infected mice was assessed by Evans blue exclusion assay, as described (Torre et al., 2015). Briefly, mice were injected with 0.2mL of 1% Evans blue dye (Sigma Aldrich) on d6 p.i. with *Pb*A. One hour later, mice were exsanguinated and perfused with phosphate-buffered saline. Brains were then excised and incubated with dimethyl formamide for 48h to extract the dye, which was then quantified by optical density measured at 610nm.

Cellular Immunophenotyping

WT and *Bpgm*^{L166P} mice were immunophenotyped at steady state. 2.5x10^6 bone marrow and splenic cells were stained with antibody cocktails: BV421 anti-CD11b (clone: M1/70, 1:500, Biolegend), PE-Cy5 anti-F4/80 (clone: BM8, 1:400, eBioscience), PE anti-CD11c (clone: N418, 1:200, eBioscience), PerCP-Cy5.5 anti-Ly6G (clone 1A8, 1:300, Biolegend), FITC anti-Ly6C (clone: HK1.4, 1:400, Biolegend), and APC-eflouro780 anti-CD45 (clone 30-F11, 1:300, Invitrogen) for myeloid cells, and PE anti-TCRß (clone: H57-597, 1:200, eBioscience), APC anti-NKp46 (clone: 29A1.4, eBioscience), PerCP-Cy5.5 anti-CD4 (clone: RM4-5, 1:300, eBioscience), Alexa Fluor 700 anti-CD8a (clone: 53-6.7, 1:200, eBioscience), BV421 anti-B220 (clone: RA3-6B2, 1:400, Biolegend) and APC-eflouro780 anti-CD45 (clone 30-F11, 1:300, Invitrogen) for lymphoid cells. Cellular infiltration in the brain was performed on d5 p.i. with *Pb*A as previously described (Torre et al., 2017). Infiltrating cells were stained with antibody cocktails: PerCP-Cy5.5 anti-CD4 (clone RM4-5, 1:300, eBioscience), PE anti-CD8a (clone 53-6.7, 1:400, eBioscience), FITC anti-TCRß (clone H57-597, 1:200, eBioscience), BV421 anti-CD19 (clone 6D5, 1:300, BioLegend), APC anti-CD11b (clone M1/70, 1:400, eBioscience), PE anti-Ly6C (clone HK1.4, 1:3000, eBioscience), FITC anti-Ly6G (clone 1A8, 1:400, BioLegend) and APC-eflouro780 anti-CD45 (clone 30-F11, 1:400, Invitrogen). All non-viable cells were excluded using Zombie Aqua Dye-V500 (7-AAD) (1:400, Biolegend). Samples were acquired using BD LSR Fortessa and analyzed using FlowJo software (Tree Star).

EPO Quantification

Serum erythropoietin (EPO) was quantified by mouse EPO ELISA kit following the manufacturer's instructions (R&D system, MEP00B).

Treatment with Phenylhydrazine

Hemolytic anemia was experimentally induced with one dose of neutralized phenylhydrazine (Sigma-Aldrich) at a concentration of 50mg/kg. Erythroid parameters were analyzed at d5 post-treatment and were performed as described above.

Metabolite Profiling

Authentic standards were obtained from Sigma Aldrich where possible. 1,3-Bisphosphoglyceric acid was synthesized as described (Oslund et al., 2017), but not purified. It was used to determine retention time compared to 2,3-Bisphosphoglyceric acid. Water, methanol, acetonitrile, acetic acid and tributylamine were obtained from Fischer Scientific. Metabolites were profiled at the Rosalind and Morris Goodman Cancer Research Centre Metabolomics Core Facility. Blood was collected in EDTA coated tubes (Sarstedt) from WT and *Bpgm*^{L166P} mice. Cells were washed with saline and centrifuged to remove the supernatant. Polar metabolites were extracted by adding 500μL 80% MeOH, vortexing the samples for 1 minute and centrifuging at 21,130.2 x g for 10 minutes at 1°C. The supernatant was transferred to a microcentrifuge tube and dried by using a chilled vacuum centrifuge operating at a sample temperature of - 4°C (Labconco). Samples were resuspended in 50 μL of HPLC-grade water before LC-MS analysis. For targeted metabolite analysis, samples were injected onto an Agilent 6470 Triple Quadrupole (QQQ)–LC–MS/MS. Chromatographic separation of metabolites was achieved by using a 1290 Infinity ultra-performance quatrinary pump liquid chromatography system (Agilent Technologies. The mass spectrometer was equipped with an electrospray ionization source, and samples were analyzed in negative mode.

Multiple reaction monitoring parameters (qualifier/quantifier ions and retention times) were obtained from the Agilent MRM database and optimized using authentic metabolite standards. The quantifying and qualifying ion transitions for both 2,3-BPG and 1,3-BPG were 264.9→166.9 and 264.9→79.0, respectively. Using this method, 1,3-BPG elutes at 16.6 min, while 2,3-BPG elutes at 17 min. The source-gas temperature and flow were set at 150 °C and 13 L min^{-1}, respectively, the nebulizer pressure was set at 45 psi, and capillary voltage was set at 2,000 V. Chromatographic separation of the isomers and other meatabolites was achieved by using a Zorbax Extend C18 column 1.8 μm, 2.1 × 150mm^2 with guard column 1.8 μm, 2.1 × 5mm^2 (Agilent Technologies). The chromatographic gradient started at 100% mobile phase A (97% water, 3% methanol, 10 mM tributylamine, 15 mM acetic acid, 5 μM medronic acid) for 2.5 min, followed with a 5-min gradient to 20% mobile phase C (methanol, 10 mM tributylamine, 15 mM acetic acid, 5 μM medronic acid), a 5.5-min gradient to 45% C and a 7-min gradient to 99% C at a flow rate of 0.25 mL min^{-1}. This was followed by a 4-min hold time at 100% mobile phase C. The column was restored by back-washing with 99% mobile phase D (90% ACN) for 3 min at 0.25 mL min^{-1}, followed by increase of the flow rate to 0.8 mL min^{-1} over 0.5 min and a 3.85-min hold, after which the flow rate was decreased to 0.6 mL min^{-1} over 0.15 min. The column was then re-equilibrated at 100% A over 0.75 min, during which the flow rate was decreased to 0.4 mL min^{-1}, and held for 7.65 min. One minute before the next injection, the flow was brought back to forward flow at 0.25 mL min^{-1}. For all LC–MS analyses, 5 μL of sample was injected. The column temperature was maintained at 35°C. Relative concentrations were determined from external calibration curves. Data were analyzed by using MassHunter Quantitative Data Analysis B.10.00 (Agilent Technologies). No additional corrections were made for ion suppression; thus, concentrations are relative, not absolute.

QUANTIFICATION AND STATISTICAL ANALYSIS

Graphs, pathway analyses, heatmaps, and all statistical tests were performed using GraphPad Prism 6.0 (GraphPad Software, Inc, La Jolla, CA). Analyses were performed using Mantel-Cox log-rank, Sidak's multiple comparison or two-tailed unpaired Student's t test as indicated in the figure legends. Statistical significance was considered as a *p-value* of $p < 0.05$. For all animal experiments an individual mouse was considered a biological replicate. A minimum of 5 animals were used per experiment with a minimum of two-independent experiments performed. "n" represents the number of animals. Individual data points with means and standard deviations are shown for all dot plots. No data points were excluded. FlowJo software was used to visualize and quantify all FACS data. MetaboAnalyst 3.0 (Xia et al., 2015) was used to analyze all metabolomics' data. Representative contour plots are shown in Figures 3, 4, 6, S2, S3, and S6.